J Neurophysiol 118: 2770–2788, 2017.
First published September 6, 2017; doi:10.1152/jn.00455.2017.

RESEARCH ARTICLE | *Sensory Processing*

Tests of the sorption and olfactory "fovea" hypotheses in the mouse

David M. Coppola,[1]* Brittaney E. Ritchie,[1] and Brent A. Craven[2]*
[1]*Biology, Randolph-Macon College, Ashland, Virginia; and* [2]*Mechanical and Nuclear Engineering, The Pennsylvania State University, University Park, Pennsylvania*

Submitted 18 June 2017; accepted in final form 1 September 2017

Coppola DM, Ritchie BE, Craven BA. Tests of the sorption and olfactory "fovea" hypotheses in the mouse. *J Neurophysiol* 118: 2770–2788, 2017. First published September 6, 2017; doi:10.1152/jn.00455.2017.—The spatial distribution of receptors within sensory epithelia (e.g., retina and skin) is often markedly nonuniform to gain efficiency in information capture and neural processing. By contrast, odors, unlike visual and tactile stimuli, have no obvious spatial dimension. What need then could there be for either nearest-neighbor relationships or nonuniform distributions of receptor cells in the olfactory epithelium (OE)? Adrian (Adrian ED. *J Physiol* 100: 459–473, 1942; Adrian ED. *Br Med Bull* 6: 330–332, 1950) provided the only widely debated answer to this question when he posited that the physical properties of odors, such as volatility and water solubility, determine a spatial pattern of stimulation across the OE that could aid odor discrimination. Unfortunately, despite its longevity, few critical tests of the "sorption hypothesis" exist. Here we test the predictions of this hypothesis by mapping mouse OE responses using the electroolfactogram (EOG) and comparing these response "maps" to computational fluid dynamics (CFD) simulations of airflow and odorant sorption patterns in the nasal cavity. CFD simulations were performed for airflow rates corresponding to quiet breathing and sniffing. Consistent with predictions of the sorption hypothesis, water-soluble odorants tended to evoke larger EOG responses in the central portion of the OE than the peripheral portion. However, sorption simulation patterns along individual nasal turbinates for particular odorants did not correlate with their EOG response gradients. Indeed, the most consistent finding was a rostral-greater to caudal-lesser response gradient for all the odorants tested that is unexplained by sorption patterns. The viability of the sorption and related olfactory "fovea" hypotheses are discussed in light of these findings.

NEW & NOTEWORTHY Two classical ideas concerning olfaction's receptor-surface two-dimensional organization—the sorption and olfactory fovea hypotheses—were found wanting in this study that afforded unprecedented comparisons between electrophysiological recordings in the mouse olfactory epithelium and computational fluid dynamic simulations of nasal airflow. Alternatively, it is proposed that the olfactory receptor layouts in macrosmatic mammals may be an evolutionary contingent state devoid of the functional significance found in other sensory epithelia like the cochlea and retina.

computation fluid dynamics; electroolfactogram; olfactory epithelium

IN ANIMALS with advanced nervous systems, arrays of specialized sensory receptor cells in the eye, skin, cochlea, mouth, and nasal cavity transduce environmental information about light, mechanical forces, sound, and environmental chemicals. The receptive ranges of these sensory cells have been shaped by natural selection to detect stimuli with reliable relevance for survival. Efficiencies in information capture accrue by allocating receptors nonuniformly in time and space. The retinal fovea of primates, with its concentration of cone receptors placed at the center of gaze; the tactile fovea of certain fossorial mammals, with its high concentration of primary somatosensory afferents innervating a specialized nasal appendage; and the cochlear fovea of some bats, with a concentration of hair cells tuned to the frequency of the animal's echolocation calls, provide salient examples of this adaptation (Catania 2011; Osterberg 1935; Suga et al. 1975). In these instances, natural selection has clustered receptor cells in strategic locations to increase information capture.

Intriguingly, it has also been postulated that the olfactory system of rodents (and presumably other macrosmatic mammals) may possess a fovea-like distribution of receptors with associated behaviors designed to direct odors to "foveal" or extrafoveal locations on the olfactory epithelium (OE; Schoenfeld and Cleland 2005, 2006). This hypothesis is based on three propositions: first, that there exists a nonuniform distribution of receptor densities and ratios of convergence along a central to peripheral trajectory in the rodent olfactory mucosa, likened to the retina's nonuniform distribution of photoreceptors; second, that odor selectivity (receptive range) of olfactory receptors differs systematically between the central (defined as the dorsal recess) and peripheral (defined as lateral and ventral regions) OE analogous to the dichotomy between retinal rods and cones; and third, that sniffing strategies—"olfactory saccades"—can direct odors to their corresponding receptor populations centrally or peripherally (Schoenfeld and Cleland 2005).

The present study deals with the second and third of these propositions. These ideas have a long history in chemosensory research dating back to Adrian's (1950) demonstration that odorants with high solubility caused larger responses in olfactory nerves innervating rostral parts of the nasal cavity, and, conversely, that odorants with high volatility (low solubility) caused larger responses ventrally. This observation prompted Adrian to speculate that olfactory coding, consonant with the other special senses, may have a spatial component based on odor solubility, an idea commonly referred to today as the "sorption hypothesis" (Cenier et al. 2013). Sorption refers to a number of physical characteristics, including water solubility,

* D. M. Coppola and B. A. Craven contributed equally to this work.

Address for reprint requests and other correspondence: D. M. Coppola, Department of Biology, Randolph-Macon College, Ashland, VA 23005-5505 (e-mail: dcoppola@rmc.edu).

that influence the interaction of odorants with the olfactory mucosa as air flows through the nasal cavity during normal respiration or sniffing (Scott et al. 2014).

In the decades since Adrian's original formulation, the sorption hypothesis has garnered considerable support and further elaboration. Mozell and colleagues in a series of studies firmly established that the nasal cavities of amphibians, rats, and humans function like the stationary phase of a gas chromatograph, separating odors that flow through them (Kent et al. 1996; Kurtz et al. 2004; Mozell 1964, 1966, 1970). And a clear distinction has been recognized between what is termed the "imposed" pattern of odor stimulation of the OE based on differential sorption (i.e., the chromatographic effect) and the "inherent pattern" of odor responses based on the spatial distribution of olfactory receptors with distinctive receptive ranges (Kent et al. 1996; Moulton 1976). Supporting this dichotomy, Scott and colleagues have repeatedly shown in the rat that both an imposed and an inherent pattern of odor responsivity exist across the OE that comports with the sorption hypothesis (Scott 2006; Scott et al. 1996, 2000, 2014). Moreover, different olfactory receptor types appear to be distributed, with few exceptions, in a central to peripheral fashion—a layout purportedly consistent with the inherent pattern needed to support sorption as a coding mechanism (Iwema et al. 2004; Miyamichi et al. 2005; Ressler et al. 1993; Sullivan et al. 1996).

Contrary to this corpus supporting the sorption hypothesis, we recently mapped the inherent pattern of olfactory responses in the mouse OE using the electroolfactogram (EOG) and found little support for the notion (Coppola et al. 2013). In particular, while we observed large regional differences in OE responses, which were odor specific, some water-soluble odorants and highly insoluble odorants gave similar patterns of response across the sampling area that included central and peripheral recording sites. However, this study included only a relatively small number of odorants with sampling limited to the medial surface of the endoturbinates. In the present study, we have again used the EOG but here included a larger set of odorants at the extremes of sorptiveness as well as lateral-peripheral and ventral-peripheral recording sites. Critically, we also performed computational fluid dynamics (CFD) simulations of airflow and odorant sorption in the mouse nasal cavity for comparison with the inherent pattern of responses. Our results provide, to our knowledge, among the first evidence in any mammal besides the rat that highly sorptive odorants produce a larger response centrally than peripherally across the OE consistent with one prediction of the sorption hypothesis. However, highly insoluble odorants did not cause greater responses in the periphery than centrally as predicted by the sorption idea and there was a marked difference between ventral and lateral (both peripheral locations) response profiles. Finally, as in our previous study, we confirmed that the most pronounced spatial inhomogeneity in odor responses was a rostral-greater to caudal-lesser gradient that was observed for high-sorption and low-sorption odors alike and was uncorrelated with odor sorption gradients from our CFD simulations.

MATERIALS AND METHODS

Animals. All animal procedures were approved by the Randolph-Macon College Internal Animal Care and Use Committee and conformed to the NIH guidelines for care and use of laboratory animals. Eighty-seven female, CD-1, adult mice (Charles River Laboratories, Wilmington, MA) were used in three experiments. Only female mice were used to minimize size differences between subjects. However, preliminary studies (data not shown) confirmed that similar results can be found in both sexes. Subjects were generally 50–90 days old at the time of use, but mice of ages up to 4 mo were included. Mice were housed three or four per cage (191 × 292 × 127 mm) in the Randolph-Macon College animal facility with ad libitum access to food and water under a 12:12-h light cycle. Recordings were performed during all phases of the lights-on period.

Surgical preparation. Immediately before electrophysiological recording mice were killed with a lethal dose of Nembutal (70 mg/kg ip). Following decapitation, a disposable microtome blade was used to separate the left and right halves of the skull along the midsagittal plane. Both hemisections of the skull were used for recording responses to odors. For experiments directed at the turbinates, the nasal septum and overlying mucosa were resected to reveal the medial aspect of endoturbinates II_d, II_v, III, and IV (Fig. 1). For experiments directed at the ectoturbinates the endoturbinates were also carefully resected to reveal these former structures in the lateral recesses of the nasal cavity (we follow the common convention of using Roman numerals to designate endoturbinates and Arabic numerals for ectoturbinates). Immediately after surgery, the preparations were maintained in a humidified chamber until recordings were completed. Room temperature was maintained below 20°C to preserve the viability of the preparation.

Recording setup. Recording procedures have been described previously (Barber and Coppola 2015; Coppola et al. 2013). Briefly, recordings took place within a Faraday cage covered with plastic sheeting. The chamber was suffused with the output of an ultrasonic humidifier and a forced-air humidifier that increased humidity near the preparation and maintained positive pressure. Humidity measurements, taken in the vicinity of the preparation during recording sessions, were never less than 98%.

Once the preparation was immobilized in the recording chamber a recording electrode was positioned at predetermined locations on the medial surface of the endoturbinates, ectoturbinates, or septal mucosa under microscopic guidance using a three-axis manipulator (Fig. 1). For reasons discussed previously, a single electrode was repeatedly repositioned until all of the target locations were recorded from for a given subject (Coppola et al. 2013). The stimulation port was also moved for every recording site with care taken to place it at the same distance and angle to the recording electrode. For all recordings, the tip of the indifferent electrode was placed on the frontal bone at its intersection with the cribriform plate and immobilized with a magnetic clamp. The recording electrodes consisted of Ag/AgCl wires inside glass capillaries that had been pulled to ~50 μm tip diameter and filled with 0.05% agar in 0.1 M PBS. The indifferent electrodes consisted of Ag/AgCl wire inside a 500-μl pipette tip filled as above. Electrodes were connected to the inputs of an Iso-DAM8A DC Amplifier (World Precision Instruments, Sarasota, FL) with low-pass filtering set at 10 Hz. The output of the amplifier was sampled at 20 Hz by a PowerLab/8SP (AD Instruments, Colorado Springs, CO), which provided analog-to-digital conversion, display, and recording. The dependent variable in all experiments was the EOG maximum amplitude, measured semimanually for each trace with the use of the LabChart software within PowerLab.

Stimulation setup. Odors were delivered to the mucosal surface in a 0.5-s pulse of air (700 ml/min) from the headspace above a 10-ml mixture of odorant dissolved in mineral oil (for all but vanillin) contained in a 25-ml vial. The carrier gas was charcoal-filtered room air that was humidified before entering the stimulus apparatus. A custom unit consisting of computer, software, interface, and olfactometer (Knosys, Lutz, FL) controlled stimulus duration and timing. However, odor type and concentration were selected by manually switching the reservoir vial that was in line with the odor port. The

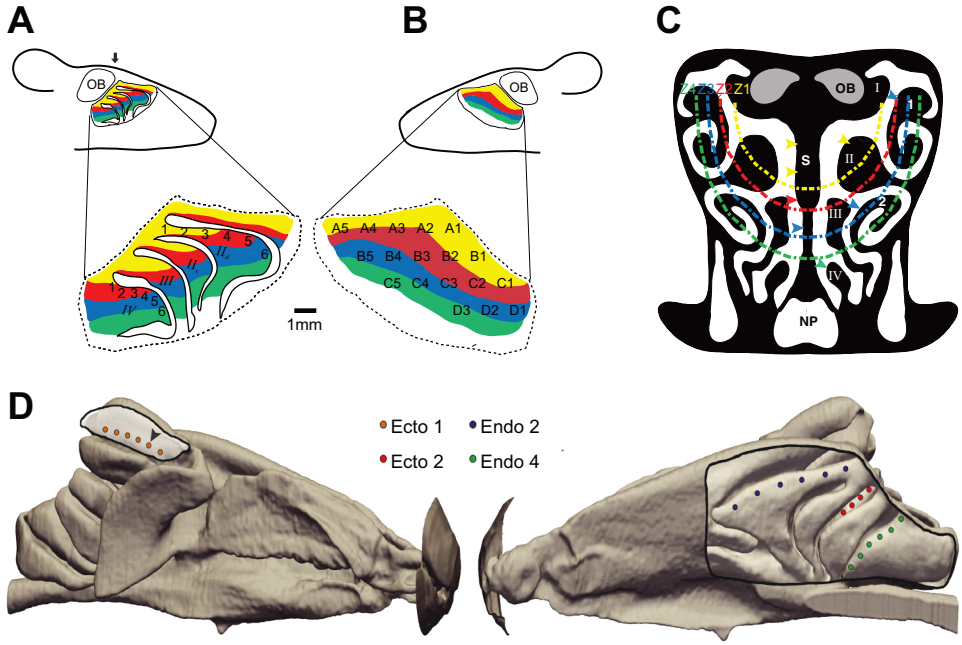

Fig. 1. Electroolfactogram (EOG) recording locations on the olfactory epithelium (OE) of the mouse nasal cavity. *A*: drawing of midsaggital view of left olfactory endoturbinates with septum resected. There are 6 recording locations (1–6), 1 mm apart, along endoturbinate II_d near to its dorsal border. There are 6 recording locations (1–6), 0.5 mm apart, along endoturbinate IV near its dorsal border. Colors correspond to the approximate locations of classical receptor zones in the mouse (Ressler et al. 1993). *B*: drawing of midsaggital view of left septum showing grid of 18 recording locations. As in *A*, colors depict approximate borders of classical receptor zones (Ressler et al. 1993). *C*: drawing of coronal section through the nasal cavity at the approximate the rostrocaudal location shown by arrow in *A*. Colored dashed lines show approximate peripheral borders of classical receptor zones (Login et al. 2015). The "central" designation throughout the text refers to zone 1 while the "peripheral" designation refers to zones 2–4. Colored arrowheads mark approximate recording locations on turbinates (*experiment 2*) and septum (*experiment 3*). Roman numerals label endoturbinates; Arabic numbers label ectoturbinates; d, dorsal; v, ventral; OB, olfactory bulb; S, nasal septum; NP, nasopharynx. *D*: anatomically accurate computational fluid dynamics (CFD) model of the right nasal airway of the mouse. Values of odorant flux were extracted from CFD simulations of odorant deposition during quiet breathing and a quasi-steady sniff at the same approximate locations as EOG recording measurements on each turbinate, illustrated here with circular symbols. In the medial view (*right*), the septum has been digitally removed to reveal the ethmoturbinates and the EOG recording locations on ectoturbinate 2 and endoturbinates II_d and IV. In the lateral view (*left*), ectoturbinate 1 was likewise partially digitally resected to reveal the EOG recording locations. *Experiment 1* recording locations are designated with arrowheads. Ectoturbinate 1 recording locations are actually on the medial surface; thus *D* is a transparent view.

interstimulus interval was held to a minimum of 50 s for all experiments.

The odor delivery port consisted of a 3-cm-long, 3.5-mm-diameter glass tube connected by a 3-cm-long Teflon tube to the odor reservoir vial. A three-axis micromanipulator was used to position the odor port 10 mm from the point at which the recording electrode made contact with the OE. A rigid guide hair affixed to the end of the odor port was used to maintain a consistent standoff distance and angle (45–55°) in relation to the surface of the OE.

The stimuli used in this study were all single molecules at or near the highest purities (>97% to >99%) commercially available (Sigma-Aldrich). Odorants were selected that *1*) had been used previously in olfactory physiological and psychophysical studies, *2*) included a range of odor qualia, and, *3*) most critically, spanned a wide range sorptiveness values, the latter character measured by mucus and water solubility (Schoenfeld and Cleland 2005, 2006; Scott et al. 2014).

For the sake of clarity and brevity, the highly sorptive molecules used in this study will be referred to as "soluble" and the weakly sorptive molecules will be referred to as "insoluble." For *experiment 1*, isoamyl acetate was used as a standard for comparison to 10 highly soluble odorants (Fig. 2) and 10 highly insoluble odorants (Fig. 3) that were selected from a stimulus set recently used by Scott and colleagues (2014) in a study of the sorption hypothesis in rats. As argued in that publication, water solubility does not completely capture the parameter of "sorptiveness" as regards interaction of an odorant with the OE. Thus the set of 20 odors used here were selected because they are at the low and high extremes of air/mucus partition coefficients (see derivation in Scott et al. 2014).

For *experiments 2* and *3*, the stimulus set consisted of three odorants including a water-soluble odorant, acetophenone (5.5 g/l water solubility); a less soluble odorant, isoamyl acetate (2 g/l water solubility); and a very slightly soluble odorant, nonane (0.0002 g/l water solubility). The air-mucus odorant partition coefficients (2.11×10^{-4} for acetophenone, 5.31×10^{-3} for isoamyl acetate, and 0.509 for nonane) for these stimuli were calculated as described by Rygg et al. (2017; water solubility estimates from United States Environmental Protection Agency's EPI Suite). Acetophenone was chosen in these experiments rather than some of the more water-soluble odorants used in *experiment 1* because it has repeatedly been shown to evoke decreasing inherent responses from the OE as one moves recording locations down the airstream path in the rat nasal cavity (reviewed by Scott 2006). Moreover, Rygg and colleagues (2017) have recently shown that choosing an odor with mucus solubility greater than that of acetophenone makes a negligible difference in the CFD-simulated sorption pattern within the nasal cavity.

For all odors, the exact concentrations delivered to the OE were undetermined as they were immaterial to the goals of this study. Stimuli were prepared as the 0.1% vol/vol dilution of odor in mineral oil except for nonane in *experiments 2* and *3* that was prepared at 5.0% vol/vol dilution and vanillin in *experiment 1* which was used in undiluted solid form (headspace above 2 mm sphere). Importantly, our use of a single odor concentration is justified by our previous study of mice (Coppola et al. 2013) and work by other laboratories with rats (Scott and Brierley 1999), which established that spatial patterns of EOG responses remain nearly constant despite changes in stimulus concentration except near the threshold or ceiling of the

Odor	Log Air/Mucus Partition[1]	MW	Structure
Vanillin	-7.1910	152	
1-Methyl-2-Pyridone	-5.9962	109	
Methyl Isonicotinate	-5.7353	137	
Octanoic Acid	-5.7213	144	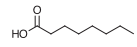
Heptanoic Acid	-5.4656	130	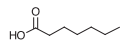
p-Anisaldehyde	-4.9669	136	
Menthol	-4.7082	156	
(S)-(-)-Perillyl Alcohol	-4.6035	152	
Ethylacetoacetate	-4.3132	130	
Ethyl Benzaldehyde	-4.1900	134	

Fig. 2. Highly soluble odorants used as stimuli in *experiment 1A* and *1B* with air/mucus partition coefficients, molecular weights (MW), and chemical structures.

response range. The 0.1% concentration used for most of this and our previous study (Coppola et al. 2013) represents approximately the upper third quartile of EOG response magnitudes for isoamyl acetate, the odor from our panel that triggered the strongest response at most loci on the OE. Finally, pilot studies (data not shown) using several odorants established that the 0.1% concentration for most odors and the 5.0% concentration for nonane were well above the EOG response threshold and well below the maximum EOG response for each odor.

Experimental designs. Owing to the variability of the EOG response, especially its rundown due to both time and response fatigue, some investigators have used the technique of normalizing responses, often to a standard odorant such as amyl acetate (e.g., Mackay-Sim and Kesteven 1994; Scott and Brierley 1999). However, our previous study of EOG responses in the mouse OE established a marked anterior-larger to posterior-smaller gradient to isoamyl acetate and other odorants. This gradient would create a substantial bias in a standardized response variable depending on how the procedure is performed. Therefore, our preferred method has been to use randomization and replication to overcome the inherent imprecision of the EOG (Barber and Coppola 2015; Coppola et al. 2013; Waggener and Coppola 2007). However, because of the extensive number of odorants (11) in *blocks A* and *B* of *experiment 1* (see below), EOG responses are reported as percentages of the isoamyl acetate response, most proximate in time at the same location. This standardization procedure was designed to minimize differences in EOG amplitudes due to rundown in response (Scott et al. 1996) even though previous control experiments established that such rundown is minimal ($< 5\%$) for the first 10 stimulations of a particular OE recording site (Barber and Coppola 2015).

For *experiment 2* we used our preferred method of reporting raw EOG amplitudes while for *experiment 3*, which focuses on the overall 2D pattern of responses in the septum, data are reported as percentages of the maximum response across the recording grid for each odorant.

In *experiment 1*, only one recording location was used on each of three turbinates: II_d, IV, and 1 owing to the relatively large number of stimuli (12 each for *blocks A* and *B*). The recording locations correspond to the 2nd most rostral standard location as shown in Fig. 1*D*. These locations were chosen because they tended to be at or near the most responsive locations for each turbinate.

The 20 odors listed in Tables 1 and 2 were divided into two groups of five highly soluble odorants and five highly insoluble odorants forming *blocks A* and *B*. At each recording location, the standard odorant isoamyl acetate was always the 1st and the 7th stimuli with test odorants taking the 2nd to 6th and 8th to 12th positions in the stimulus sequence. Stimulus ordering was otherwise counterbalanced such that each test odor took various positions when considered over the entire experiment.

In *experiment 2*, EOGs were recorded at 1-mm intervals (six locations) along the medial face of endoturbinate II_d near its dorsal edge, at 0.5-mm intervals (six locations) along the medial face of endoturbinate IV near its dorsal edge, and at 0.5-mm intervals along a rostrocaudal axis in the dorsoventral center of ectoturbinate 1 (six locations) and ectoturbinate 2 (four locations; see Fig. 1). Distances between recording locations are nominal for the EOG recordings and the CFD simulations (see *Computational fluid dynamics* below) since the actual intervals varied due to differences in animal size.

In *experiment 2A*, turbinates II_d, IV, and 1 were recorded by repeated measures in the same animal using only one of the three

Odor	Log Air/Mucus Partition[1]	MW	Structure
Methyl Butyrate	-2.2616	102	
Methyl Propionate	-2.1519	88	
D-Limonene	-2.1164	136	
Alpha Pinene	-1.3141	136	
Vinyl Cyclohexane	-0.9878	110	
Cyclohexane	-0.7389	84	
Octane	-0.4943	114	
Heptane	-0.3753	100	
Decane	-0.1829	142	
Hexane	0.0532	86	

Fig. 3. Highly insoluble odorants used as stimuli in *experiment 1A* and *1B* with air/mucus partition coefficients, molecular weights, and chemical structures.

odorants for each animal (n = nine animals for each odor). In *experiment 2B*, turbinate 2 responses were measured using three odors at each of four locations (n = 14 animals). In *experiment 3*, a trapezoidal grid of 18 recording locations on the OE of the septum was targeted (Fig. 1*C*). The recording locations were 1 mm apart and formed four rows of five, five, five, and three sites, respectively, that ran in an approximately rostral-caudal axis. This configuration allowed sampling of virtually the entire surface of the OE on the septum. Only one odor was used per subject and recordings were ordered by location in a randomized fashion (without replacement).

The sampling scheme discussed above was informed by previous estimates of the spatial resolution of EOG recordings which is a function of the electrical space constant of the OE and spread of odorant from the recording electrode. Mackay-Sim and Kesteven (1994) combined measurements of both parameters in rat OE to determine that 95% of the EOG response was accounted for by olfactory sensory neurons (OSNs) within ~0.3 mm of the recording electrode dropping exponentially with distance.

Statistical analysis. Data were analyzed using Prism 6 (GraphPad Software, La Jolla, CA) with alpha set at $P < 0.05$. EOG amplitude was the dependent variable and recording location was the independent variable for all experiments. In *experiment 1*, EOG amplitudes standardized to the most recent isoamyl acetate response were used for all analyses. For *experiment 2*, raw EOG amplitudes were used for the analysis. *Experiment 3* was descriptive and thus no statistical analyses were performed with the exception of the septum and turbinate response comparisons for which raw EOG amplitudes were used.

In *experiment 1*, the ratio data, scaled to the isoamyl acetate responses at each location, passed the D'Agostino-Pearson omnibus normality test implemented in Prism. Therefore, a two-way repeated-measures ANOVA, with odor and turbinate as main effects, were used to analyze these data. The ANOVAs were followed by Tukey's multiple-comparison test, as implemented in Prism 6, to determine P values for pairwise comparisons. Additionally, data from *experiment 1* were plotted as ratios of central (endoturbinate II) to peripheral (endoturbinate IV or ectoturbinate 1) responses in the OE vs. air/mucus solubility. The nonparametric analyses used to analyze certain aspects of these data are described in the RESULTS section.

For *experiment 2*, two-way repeated-measures ANOVAs were used to assess differences between EOG responses with recording location (within-subject variable) and odor (between-subject variable) as the main effects. Given that our previous study found a significant rostral-greater to caudal-lesser gradient of responses, tests for a linear trend across locations were performed (Coppola et al. 2013). Finally, to compare responses among turbinates and the septum, data were collapsed across locations providing between-subject grand means and SEs. These data were compared by a standard one-way ANOVA followed by Tukey's multiple-comparison tests.

Computational fluid dynamics. CFD simulations of airflow in the right nasal airway of a mouse (38.8 g CD-1 strain female, Charles River Laboratories) were performed using the computational model developed in our previous study (Coppola et al. 2014). Briefly, high-resolution (25 μm isotropic) MRI scans were acquired at Pennsylvania State University and used to reconstruct an anatomically accurate model of the airway using the methodology of Craven and colleagues (Craven et al. 2007; Ranslow et al. 2014). Owing to the bilateral symmetry of the airway in the present specimen, only the right nasal airway was reconstructed. Furthermore, based on our previous study (Coppola et al. 2014), which included anatomical

Table 1. *Two-way ANOVAs of EOG magnitude from experiment 2*

Source	SS	df	MS	*F*	*P*
			Endoturbinate II_d		
Odor	813.7	2	406.8	36.23	<0.0001
Location*	192.2	5	38.44	16.83	<0.0001
Interaction	54.18	10	5.418	2.372	<0.0134
Subjects	269.5	24	11.23	4.916	<0.0001
Residual	274.1	120	2.284		
			Endoturbinate IV		
Odor	294.4	2	147.2	9.031	<0.0012
Location*	396.5	5	79.3	18.68	<0.0001
Interaction	172.1	10	17.21	4.054	<0.0001
Subjects	391.2	24	16.30	3.840	<0.0001
Residual	509.4	120	4.245		
			Ectoturbinate 1		
Odor	213.1	2	106.6	5.327	<0.0122
Location*	181.6	5	36.33	13.61	<0.0001
Interaction	148.1	10	14.81	5.552	<0.0001
Subjects	480.1	24	20.00	7.496	<0.0001
Residual	320.2	120	2.669		
			Ectoturbinate 2		
Odor*	22.32	2	11.16	21.62	<.0001
Location*	14.37	3	4.789	0.5739	=0.6356
Interaction	2.791	6	0.4651	2.576	<0.0250
Subjects	216.0	13	16.61		
Residual	14.08	78	0.1806		

*Within-subjects factor. See Fig. 8. EOG, electroolfactogram; SS, sum of squares; df, degrees of freedom; MS, mean squares.

examination and morphometric analysis of multiple specimens, we determined that the nasal anatomy of the present specimen is generally representative of the mouse.

Given the reconstructed model of the right nasal airway, a high-fidelity hexahedral-dominant unstructured CFD mesh containing ~18 million computational cells was generated using OpenFOAM (version 2.4) and boundary conditions were assigned as in previous work (Coppola et al. 2014; Craven et al. 2009). Steady-state CFD simulations were performed using OpenFOAM to predict nasal airflow and odorant deposition patterns during quite breathing and a quasi-steady sniff. As recently demonstrated by Rygg et al. (2017), steady-state CFD simulations of quasi-steady airflow and odorant deposition may be used to reasonably predict time-averaged nasal airflow and odorant deposition during unsteady sniffing in the nose of animals as large as a coyote (*Canis latrans*), where the maximum Womersley number (a nondimensional parameter used to quantify the degree of unsteadiness) is in the 3–4 range. The maximum Womersley number in the mouse is much less than one, indicating that unsteady flow effects during sniffing are negligible (see Rygg et al. 2017 for further details regarding flow unsteadiness during sniffing). Accordingly, steady-state CFD simulations of laminar nasal airflow during inspiration were performed at flow rates corresponding to quiet breathing (36 ml/min; see Coppola et al. 2014) and sniffing (100 ml/min; see Challis et al. 2015). Quasi-steady odorant deposition simulations were then conducted by solving the advection-diffusion equation for odorant vapor transport with uptake at the air-mucus interface (as in Lawson et al. 2012 and Rygg et al. 2017) for three odors: acetophenone, isoamyl acetate, and nonane. An inlet odorant concentration of 1 μmol/m^3 was used for each simulation. As noted above, the air-mucus odorant partition coefficients (2.11×10^{-4} for acetophenone, 5.31×10^{-3} for isoamyl acetate, and 0.509 for nonane) were calculated as described by Rygg et al. (2017). Postprocessing and analysis of the CFD simulation results were performed using ParaView (version 5.1). Nasal airflow patterns were visualized by computing the flow streamlines from the steady-state velocity field in ParaView. Contours of odorant flux on the airway walls were visualized and quantitative values were extracted at the same approximate locations as the EOG recording measurements (Fig. 1*D*).

A CFD mesh refinement study was performed to ensure the numerical accuracy of the CFD solution. Specifically, CFD simulations were performed for the highest flow rate condition (100 ml/min) using a coarser mesh that contained 9.1 million computational cells and the qualitative and quantitative results were compared with the

Table 2. *Results from experiment 2*

Turbinate	Odor	R^2 EOG vs. Location *P* Value	*r* EOG vs. Respiration *P* Value	*r* EOG vs. Sniff *P* Value
	Acetophenone	$R^2 = 0.027$	$r = 0.066$	$r = -0.423$
		$P > 0.23$	$P > 0.90$	$P > 0.40$
Endo II_d	Isoamyl acetate	$R^2 = 0.279$	$r = 0.437$	$r = 0.109$
		$P < 0.0001$***	$P > 0.38$	$P > 0.84$
	Nonane	$R^2 = 0.094$	$r = -0.242$	$r = 0.558$
		$P < 0.03$*	$P > 0.64$	$P > 0.25$
	Acetophenone	$R^2 = 0.119$	$r = -0.350$	$r = 0.-423$
		$P < 0.01$**	$P > 0.50$	$P > 0.40$
Endo IV	Isoamyl acetate	$R^2 = 0.399$	$r = 0.049$	$r = -0.367$
		$P < 0.0001$***	$P > 0.93$	$P > 0.47$
	Nonane	$R^2 = 0.318$	$r = 0.248$	$r = -0.160$
		$P < 0.0001$***	$P > 0.63$	$P > 0.76$
	Acetophenone	$R^2 = 0.007$	$r = 0.125$	$r = -0.082$
		$P > 0.35$	$P > 0.81$	$P > 0.88$
Ecto 1	Isoamyl acetate	$R^2 = 0.220$	$r = -0.571$	$r = -0.642$
		$P < 0.0003$***	$P < 0.24$	$P > 0.17$
	Nonane	$R^2 = 0.132$	$r = -0.623$	$r = -0.611$
		$P < 0.007$**	$P > 0.19$	$P > 0.20$
	Acetophenone	$R^2 = 0.0001$	$r = 0.912$	$r = 0.431$
		$P > 0.77$	$P > 0.09$	$P > 0.57$
Ecto 2	Isoamyl acetate	$R^2 = 0.010$	$r = 0.084$	$r = 0.881$
		$P > 0.45$	$P > 0.91$	$P > 0.19$
	Nonane	$R^2 = 0.008$	$r = 0.037$	$r = 0.871$
		$P > 0.50$	$P > 0.96$	$P > 0.13$

See Fig. 8. Linear regression of EOG means on recording location and correlations between EOG means and simulated odorant flux values at each location using respiration or sniffing airflow rates. Endo, endoturbinate; Ecto, ectoturbinate. *$P < 0.05$; **$P < 0.01$; ***$P < 0.001$.

fine mesh (18 million cells) solution. The qualitative results (e.g., contours of velocity magnitude and pressure) using the coarse and fine meshes were virtually identical. Quantitatively, the induced flow rate through the nose was compared for each mesh using the same prescribed pressure applied at the nasopharynx. As discussed by Rygg et al. (2017), this quantitative measure is an excellent global metric for assessing mesh convergence. The quantitative comparison of induced nasal airflow rate showed a mere 0.2% difference between the coarse and fine mesh solutions, demonstrating that at this level of mesh resolution the CFD solution is insensitive to further mesh refinement. Accordingly, the fine mesh was used for all of the CFD simulations reported herein.

RESULTS

Experiment 1. The goal of this experiment was to directly test predictions made by the sorption hypothesis. In one interpretation of this hypothesis, olfactory receptor neurons that respond to soluble substance are assumed to be concentrated centrally (dorsal recess) and those that respond to insoluble substances are assumed to be concentrated peripherally (ventral or lateral; see DISCUSSION). Thus 10 highly mucus-soluble odors and 10 highly mucus insoluble odors, which had previously been used in a study of the sorption hypothesis, were tested along with an isoamyl acetate standard in a two block experiment (Scott et al. 2014). A single location on each of three turbinates (endoturbinate II_d, endoturbinate IV, and ectoturbinate 1) was sampled corresponding to a dorsomedial-centrally (*dmc*) positioned turbinate, a ventromedial-peripherally (*vmp*) positioned turbinate, and a dorsolateral-peripherally positioned turbinate (*dlp*), respectively (Fig. 1). These locations differ substantially both in their location—upstream to downstream—in the respiratory airflow path and in the flow rate that they experience.

The validity of the standardization to the isoamyl acetate response, employed in *experiment 1*, depended on uniform responses at the three recording locations. Though the data are not show owing to space consideration, a post hoc ANOVA analysis confirms that responses to isoamyl acetate at the three locations was not significantly different for either the first standard ($F = 0.29$, $df_{[2, 24]}$, $P > 0.6$) or the second ($F = 1.6$, $df_{[2, 24]}$, $P > 0.2$).

The omnibus ANOVAs were significant for *experiments 1A* and *1B*. However, Tukey's multiple-comparison tests are valid with or without this outcome, so only the latter probability values will be reported for brevity (Motulski 2016). Highly soluble molecules tended to evoke a greater standardized response in the central recording location than they did in either of the peripheral locations, lateral or ventral (Fig. 4, *A* and *B*). The typical pattern for the sorptive molecules was for the *dmc* responses to be significantly greater than those at both *vmp* and *dlp* locations, while the latter two locations tended to produce statistically indistinguishable responses. This was true for seven of the 10 odors in the soluble set and all of the six most-soluble odors from this group. Statistical differences emerged between the two peripheral recording locations with *vmp* displaying an intermediate response between *dmc* and *dlp* for only menthol and ethylacetoacetate, members of the soluble set from *experiment 1A*.

By contrast, normalized responses to the insoluble sets of odors did not show congruence of the two peripheral locations *vmp* and *dlp* as was the case for the soluble set, though there were much smaller differences between the responses at all three locations for the insoluble odorants compared with the soluble group. For example, methyl butyrate, methyl propionate, and D-limonene responses were statistically identical across recording locations. The significant differences that did emerge tended to be between *dlp*, displaying a higher average response, and *vmp*, displaying a lower average response, with *dmc* at an intermediate value (Fig. 4). All six of the most insoluble odorants in the set of 10 showed this pattern of responses.

To probe the relationship between an odor's sorptiveness and its OE response pattern more thoroughly, the data from *experiment 1* were converted to ratios of median responses at the central location (*dmc*) vs. the median responses at each of the two peripheral locations, *vmp* (Fig. 5*A*) and *dlp* (Fig. 5*B*). This new variable was then plotted against the log of the air/mucus partition coefficient, an accepted measure of an odor's sorptiveness (Scott et al. 2014). Note the significant negative correlation (Spearman's $r = -0.53$, $P < 0.02$) between the *dmc/vmp* ratio and air/mucus partition coefficient (PC) suggesting that the more sorptive an odor the greater the *dmc/vmp* response differential (Fig. 5*A*). In addition, the 10 values for the sorptive group in Fig. 5*A* are significantly different from the 10 values from the insoluble group (Wilcoxon matched pairs, $W = -39$, $P < 0.05$) and the ratios differ from unity (predicted under the null hypothesis) for both groups (Wilcoxon signed ranks, $W = 53$, $P < 0.004$ for solubles; $W = 41$, $P < 0.04$ for insolubles). However, both are positive values. Thus insoluble odors tend to give a greater response centrally than ventromedial-peripherally.

An even stronger negative correlation (Spearman's $r = -0.82$, $P < 0.0001$) was found between the *dmc/dlp* ratio and the PC, suggesting that the more sorptive an odor the greater the *dmc/dlp* response differential (Fig. 5*B*). Again, the 10 values for the sorptive group in Fig. 5*B* are significantly different from the 10 values from the insoluble group (Wilcoxon matched pairs, $W = -55$, $P < 0.002$) and the ratios differ from unity for both groups (Wilcoxon signed-ranks, $W = 55$, $P < 0.002$ for solubles; $W = -49$, $P < 0.01$ for insolubles). Unlike the *dmc/vmp* response differential, the *dmc/dlp* response differential showed an inversion with PC: all the soluble odorants eliciting a greater response centrally than peripherally while nine of 10 insoluble odors eliciting a greater response peripherally than centrally, though the latter difference was quite small (mean = 11%).

Experiment 2. The goal of this experiment was to compare CFD-derived odor flux values (imposed sorption patterns) with the response maps determined empirically from EOG recordings (inherent patterns) since the sorption hypothesis hinges on their correlation (see DISCUSSION). Nasal airflow patterns from the CFD simulations are used to elucidate how odors are transported through and deposited within the nose. The three odors that were used in the simulations and EOG mapping include acetophenone, isoamyl acetate, and nonane, which are highly, moderately, and slightly soluble, respectively.

Shown in Fig. 6 are airflow patterns and contours of acetophenone flux in the olfactory recess from CFD simulations of steady inspiration at flow rates corresponding to restful breathing (respiration) (Fig. 6, A_i, B_i, and C_i) and sniffing (Fig. 6, A_{ii}, B_{ii}, and C_{ii}). Gross flow patterns in the olfactory region are nearly identical for respiratory and sniffing flow rates. Air does

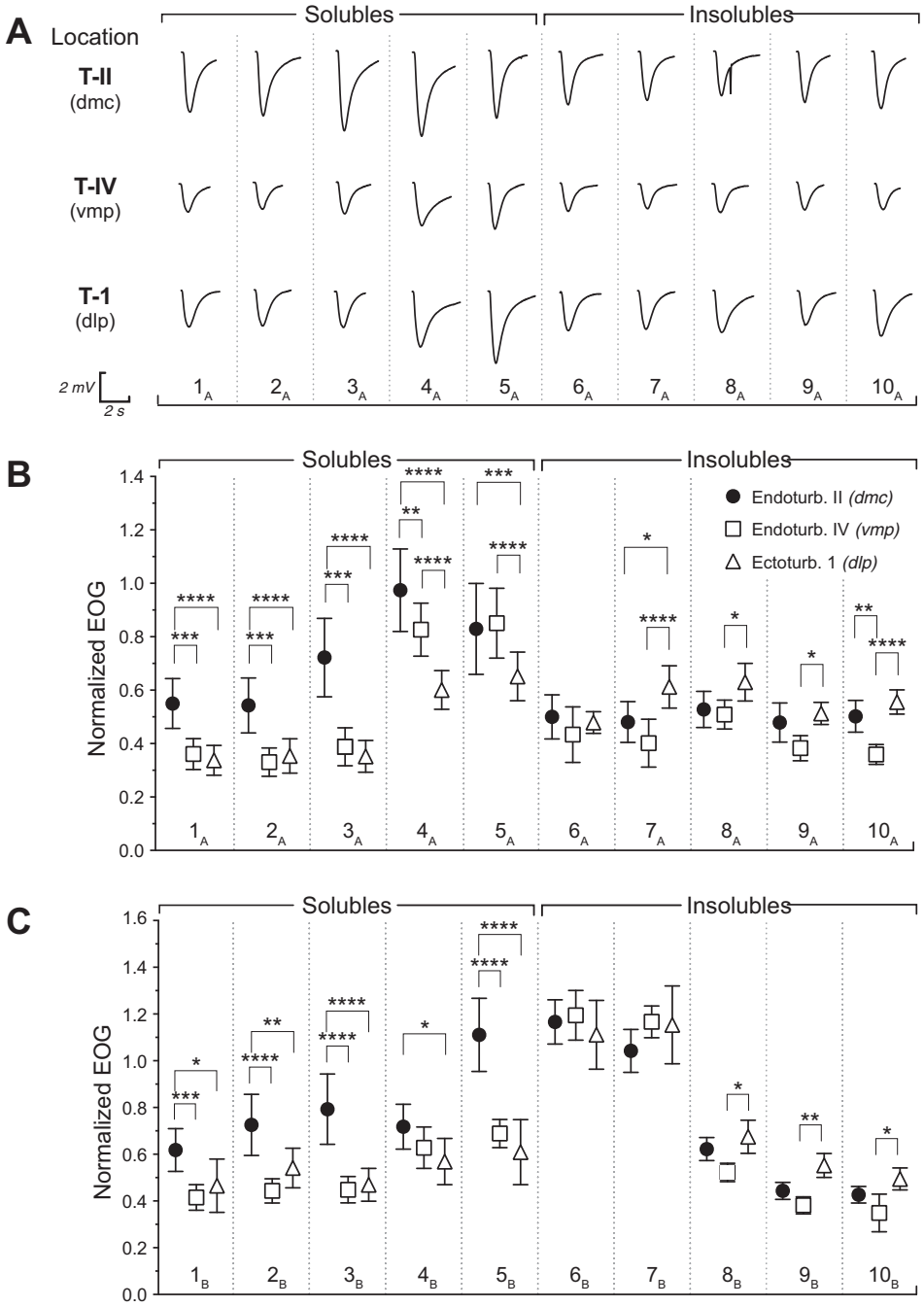

Fig. 4. *A*: raw EOG traces from 1 subject recorded at a single location on 3 turbinates: endoturbinate (Endoturb.) II_d [T-II, dorsomedial central (*dmc*)], endoturbinate IV [T-IV, ventromedial peripheral (*vmp*)], and ecoturbinate (Ectoturb.) 1 [T-1, dorsolateral peripheral (*dlp*)]. Note: larger traces centrally in response to most soluble odors and relative uniformity of insoluble odor responses. *B*: mean [± 95% confidence interval (CI)] of EOG amplitudes as a proportion of the isoamyl acetate responses using *block A* with 5 "soluble" odorants and 5 "insoluble" odorants. Odors: 1_A, vanillin; 2_A, octanoic acid; 3_A, heptanoic acid; 4_A, menthol; 5_A, ethyl acetoacetate; 6_A, D-limonene; 7_A, alpha pinene; 8_A, cyclohexane; 9_A, heptane; 10_A, hexane. *C*: mean (± 95% CI) of EOG amplitudes as a proportion of the isoamyl acetate responses using *block B* with 5 additional soluble and insoluble odorants. Odors: 1_B, 1-methyl-2-pyridone; 2_B, methyl isonicotinate; 3_B, p-anisaldehyde; 4_B, perillyl alcohol; 5_B, ethyl benzaldehyde; 6_B, methyl butyrate; 7_B, methyl proprionate; 8_B, vinyl cyclohexane; 9_B, octane; 10_B, decane. Stars above brackets illustrate significant comparisons by Tukey's multiple-comparison tests as follows: $*P < 0.05$; $**P < 0.01$; $***P < 0.001$; $****P < 0.0001$. Note: statistical results for nonsignificant comparisons were eliminated for clarity.

not flow along endoturbinate II_d in a rostral-to-caudal direction as previously assumed (Coppola et al. 2014), but rather inspired air flows into the olfactory recess via the dorsal meatus and then flows across endoturbinate II_d in a dorsal-to-ventral direction. Note that there is very little odor deposited along the rostral one-third of endoturbinate II_d. This is because the air that flows across this portion of the turbinate flowed through the medial aspect of the middle meatus and along the dorsal surface of the maxilloturbinate before entering the ventral aspect of the dorsal meatus, which feeds the olfactory recess (data not shown). Accordingly, much of the odorant in this flow stream is deposited in the maxilloturbinate region due to this upstream respiratory filtering effect (which is odorant dependent, as shown below). As a result, the acetophenone concentration in the air that flows over the rostral one-third of endoturbinate II_d is close to zero (Fig. 6, B_i and B_{ii}). And the gradient of odor flux basically consists of two regions: *1*) the rostral portion of endoturbinate II_d has a lower flux because of upstream respiratory filtering, and *2*) the caudal portion of endoturbinate II_d that has a higher flux because the odorant-laden air that passes over this portion of the turbinate flowed exclusively through the dorsal meatus, where the flow speed is higher (less residence time for odorant deposition) and there is less surface area for odorant deposition.

Air that reaches endoturbinate IV (see Fig. 1*D*) flows through the central portion of the dorsal meatus to the caudalmost extent of the olfactory recess, where it turns and flows ventrally until reaching the caudal aspect of endoturbinate IV.

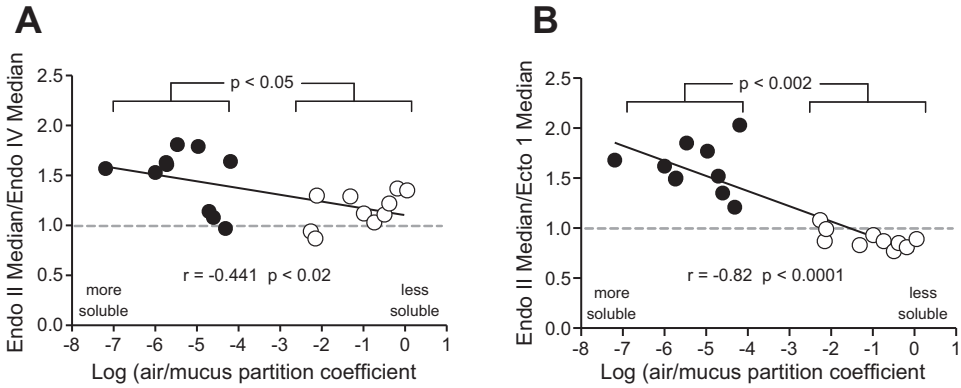

Fig. 5. Plotted are ratios of isoamyl acetate-normalized EOG response medians vs. log air/mucus solubility (see Scott et al. 2014 for derivations). *A*. shows endoturbinate II_d/endoturbinate IV response ratios (central location vs. a ventral-peripheral location). *B*, shows endoturbinate II_d/ectoturbinate 1 response ratios (central location vs. a lateral-peripheral location). Spearman correlation and associated alpha levels are provided along with the results of Wilcoxon matched pairs test to compare groups of insolubles vs. soluble odors (W, −39 for *A*; W = −55 for *B*). Also, ratios for group of 10 insolubles (white symbols) and 10 soluble odorants (black symbols) were tested for difference from unity under the null hypothesis with the signed rank test [***A*:** for soluble odors W = 53, $P < 0.004$; insolubles (less soluble) odors W = 41, $P < 0.04$; ***B*:** for soluble odors W = 55, $P < 0.002$; insolubles (less soluble) odors W = −49, $P < 0.01$].

Once it reaches endoturbinate IV, air then flows along the turbinate in a dorsocaudal to ventrorostral direction (see Fig. 6, A_i, A_{ii}, B_i, and B_{ii}). At respiratory flow rates, very little acetophenone reaches endoturbinate IV (see Fig. 6, A_i and B_i). Most of the acetophenone is deposited upstream, along the dorsal meatus. Indeed, as shown in Fig. 6B_i, the acetophenone concentration in the flow that reaches endoturbinate IV is close to zero for the respiratory flow rate case. At sniffing flow rates, however, the acetophenone vapor penetrates deeper into the olfactory recess, reaching endoturbinate IV. As shown in Fig. 6B_{ii}, there is appreciable odorant in the flow stream that reaches the caudal aspect of endoturbinate IV. As the air flows in a dorsocaudal to ventrorostral direction along endoturbinate IV, odorant is deposited, resulting in a moderate gradient of odorant flux along the turbinate in the flow direction (Fig. 6A_{ii}).

Air that reaches ectoturbinate 2 (see Fig. 1*D*) flows through the dorsal meatus to the caudal extent of the olfactory recess, where it turns and flows ventrally into the gap between endoturbinate II_d and endoturbinate III. The flow then impinges on the medial surface of ectoturbinate 2 and flows radially outward. The impingement location of this flow stream is over a broad region that extends between approximately EOG recording locations 1 and 3 (Fig. 6, B_i and B_{ii}). Note that the air that reaches ectoturbinate 2 does flow over the caudal part of endoturbinate II_d, where some of the odorant in this flow stream is deposited, particularly for the sniffing flow rate case (see Fig. 6, A_{ii} and B_{ii}). Due to the flow impinging on ectoturbinate 2 over a fairly broad region between EOG recording locations 1 and 3, there is not a significant gradient of odorant flux along this turbinate. EOG recording location 4 (the most rostral location) is the farthest from the impingement location, and it has a lower odorant flux because of this.

Air that reaches ectoturbinate 1 (see Fig. 1*D*) flows through the dorsal meatus to the caudal extent of the olfactory recess, where the flow stream turns laterally, impinges on the medial side of ectoturbinate 1, and flows around it (see Fig. 6). To reach ectoturbinate 1's recording locations, the flow impinges on the medial side of ectoturbinate 1 and flows dorsally around it; e.g., see the dorsalmost streamline in Fig. 6, A_{ii} and B_{ii}, which is the same streamline shown in the lateral view in Fig. 6C_{ii}. Air then flows in a dorsorostral direction through the meatus of ectoturbinate 1. Due to the peripheral location of ectoturbinate 1 and the low flow speeds, there is little acetophenone deposited along this turbinate during respiration. At sniffing flow rates, however, relatively more acetophenone vapor penetrates farther into the olfactory recess, reaching ectoturbinate 1. Because the flow impinges on the caudomedial side of ectoturbinate 1, there is a high odorant flux in this location (Fig. 6C_{ii}) and the magnitude of the flux decreases dorsorostrally, along the flow direction. Thus the highest odorant flux values occur at EOG recording locations 1 and 2 with a gradual decrease in odorant flux at successive recording locations (Fig. 6C_{ii}).

Surface contours of odorant flux in the olfactory recess from the CFD simulations are shown in Fig. 7 for the same three odorants used in *experiment 2*. Predictably, based on odorant sorptiveness, the upstream respiratory filtering effect on odorant deposition along the rostral portion of endoturbinate II_d is most pronounced for acetophenone (Fig. 7, A_i and A_{ii}), less so for isoamyl acetate (Fig. 7, B_i and B_{ii}), and nearly absent for nonane (Fig. 7, C_i and C_{ii}). Increasing the nasal airflow rate from a respiratory flow rate (Fig. 4, A_i, B_i, and C_i) to a sniffing flow rate (Fig. 4, A_{ii}, B_{ii}, and C_{ii}) tended to move the odorant deposition patterning farther along the airflow path (as described above) for acetophenone and isoamyl acetate but had little effect on the odorant flux pattern for nonane. The rightmost panels in Fig. 7 with the septum digitally removed to reveal the medial surface of the endoturbinates shows the area in which EOG recordings were concentrated (compare Figs. 1, 6, and 7).

While the surface contours in Fig. 7 provide useful large scale depictions of odorant sorption patterns, to test specific predictions of the sorption hypothesis a pointwise comparison between sorption patterns from CFD and EOG response maps is needed. To this end, plots of average EOG amplitudes at each recording location are juxtaposed with plots of odorant flux values at the same locations from the CFD simulations (Fig. 8). Considering the EOG data in isolation, the results replicate and extend the findings from our previous study (Coppola et al. 2013). First, in all but ectoturbinate 2, there were significant differences between average response magnitudes at different recording locations on a given turbinate (see

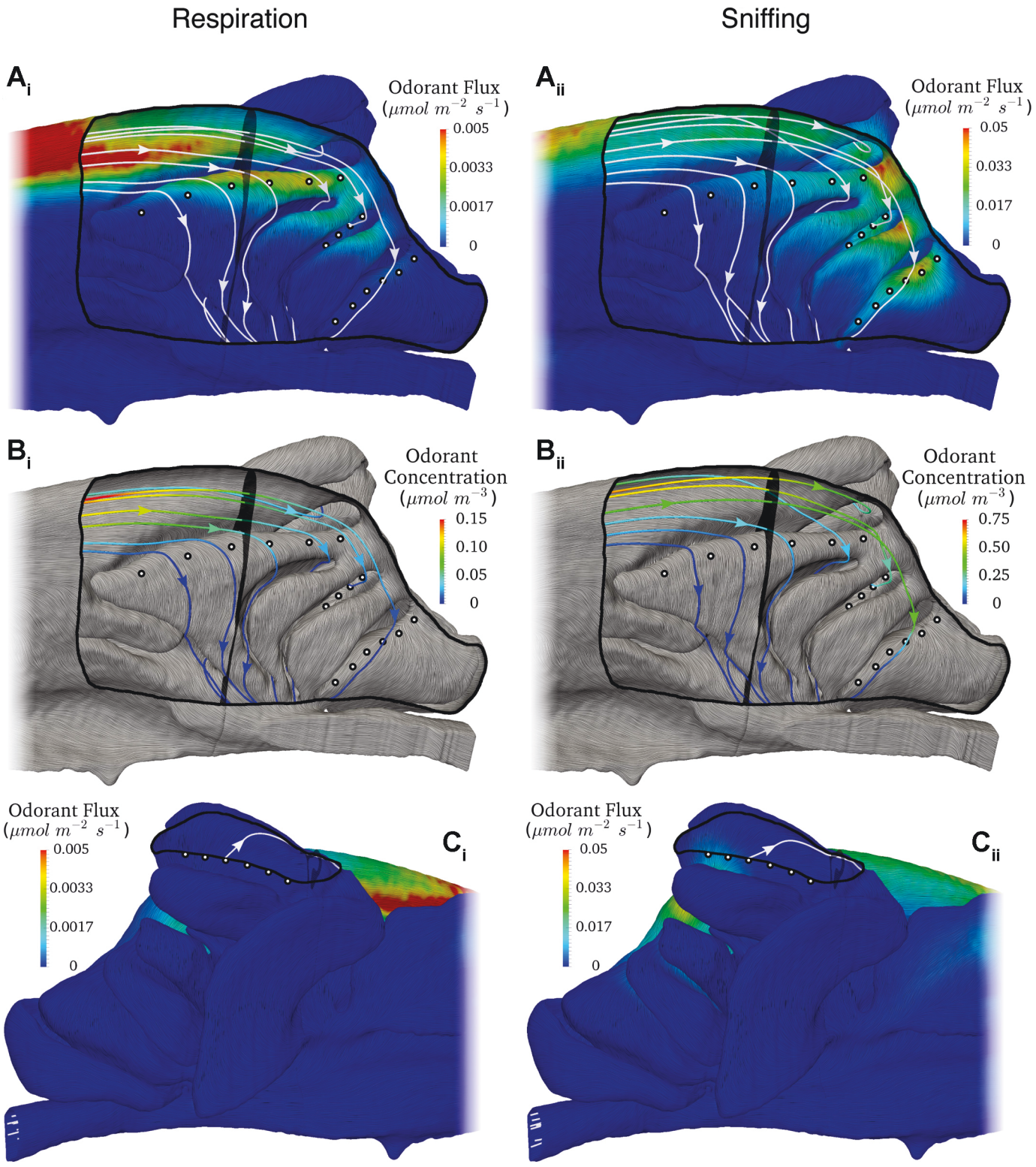

Fig. 6. Airflow and odor deposition (flux) patterns of acetophenone in the olfactory recess of the mouse from CFD simulations of steady inspiration at flow rates corresponding to respiration (A_i, B_i, and C_i) and sniffing (A_{ii}, B_{ii}, and C_{ii}). The flow patterns are illustrated using volumetric and surface-limited streamlines to show the direction of airflow in the lumen and along the walls of the airway, respectively. In the medial view (*A* and *B*), the septum has been digitally removed to reveal the ethmoturbinates and the EOG recording locations on each turbinate, illustrated with black-bordered white circles. In the lateral view (*C*), ectoturbinate 1 was likewise partially digitally resected to reveal the EOG recording locations (see Fig. 1 legend). Contours of acetophenone flux along the airway walls are shown in *A* and *C*. In *B* the volumetric streamlines are colored by acetophenone concentration and surface-limited streamlines illustrate the direction of flow along the airway walls.

ANOVA results in Table 1), which typically manifest themselves in a rostral-greater to caudal-lesser gradients of response confirmed by significant linear regressions (see R^2 values and probabilities in Table 2). Odor was a significant factor for all turbinates as was the interaction between odor and location (Table 1). Consonant with our previous study, the stimulus isoamyl acetate applied to endoturbinate IV evidenced the most dramatic gradient across recording locations with a 626%

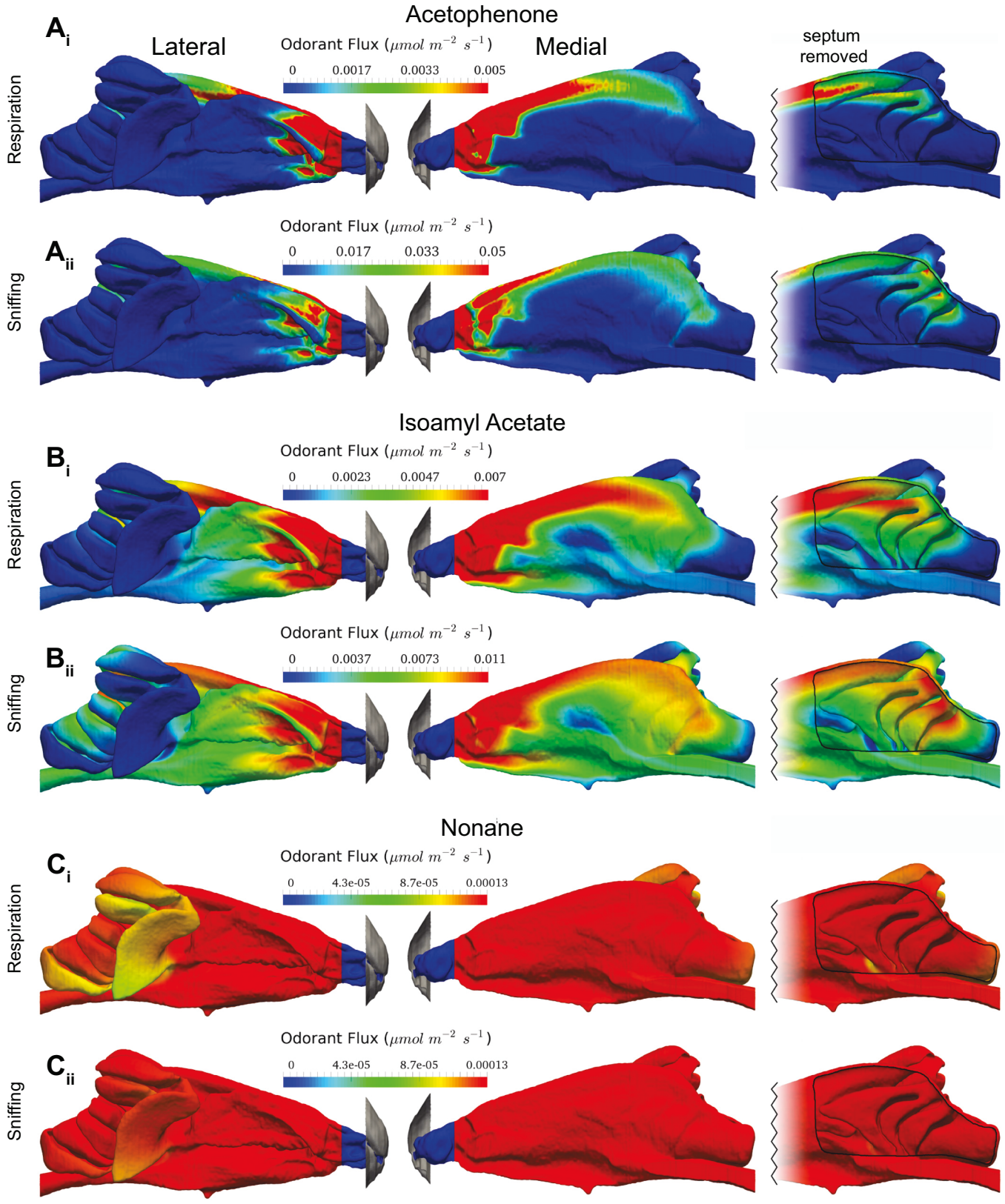

range from the least responsive location to the most responsive location. While linear fits were significant in most cases (Table 2), responses tended to drop off for the most rostral locations, consistent with our previous study, suggesting a nonlinear relationship between EOG response and rostrocaudal recording position. However, as in our previous study, there was little evidence of abrupt changes in responsiveness across locations for a given turbinate and most response patterns were well fit by a Gaussian equation (Fig. 8).

Since for ectoturbinate 2 the three odors were applied to the same subjects in a repeated measures design, a two-way repeated measures ANOVA was used to analyze these data with recording location and turbinate as the main effects. Contrary to the general result, the relatively short ectoturbinate 2 (with only 4 recording locations) showed no significant differences across recording locations for any of the three odorants ($F = 0.57$, df $_{[3, 39]}$, $P > 0.6$; see Fig. 8, *J*, *K*, and *L*). However, both odor ($F = 21.6$, df $_{[2, 26]}$, $P < 0.0001$) and the odor-location interaction were significant ($F = 2.58$, df $_{[6, 78]}$, $P < 0.025$).

Comparisons of odor sorption and odor responses gave uniform, if negative, results. No correlations between EOG amplitude and CFD-derived odorant flux values were found for either respiration or sniffing airflow rates considering all odorant-turbinate combinations (see Fig. 8 and the Pearson's *r* values in Table 2). Indeed, none of the *P* values of the correlations even approached the alpha level of 0.05. Neither did Spearman's correlation for nonlinear relationships reveal any statistically significant correlation (data not shown). A few turbinate-odor combinations are particularly instructive on this point: For example, the flux pattern of acetophenone on endoturbinate II_d reveals a steep caudal to rostral negative slope at sniffing velocities (as noted above) while the EOG responses show a caudal to rostral increase in responsivity with a dropoff at the rostral most recording location (Fig. 8*A*). In another example, the steep caudal-lesser to rostral-greater EOG profile for isoamyl acetate on endoturbinate IV (mentioned above) is matched by a rather flat odorant flux profile. These cases show that when the CFD-derived odorant flux data reveal steep gradients across recording locations on individual turbinates, the comparable EOG responses are often flat or sloping in the opposite direction. Conversely, when the EOG responses for a given odor-turbinate pairing show steep gradients they are often paired with odorant flux gradients that are relatively uniform (or sloping in the opposite direction). In general, EOG response gradients tend to be lesser-caudally to greater-rostrally and odorant flux gradients tend to be the opposite, though there are exceptions.

Experiment 3. The septal OE provides a relatively flat and continuous surface on which to study the olfactory response map. However, few studies have recorded responses in this part of the OE and we are unaware of any systematic attempt to map responses across the septum in the mouse. Thus the goal of this experiment was to determine whether there were odor specific patterns of responses on the mouse septum similar to those on the turbinates. To assess this possibility, we plotted the data as 3D surfaces with the z-axis normalized as a percent of each odor's maximum response considering all locations on the grid. For each of the three odors used in *experiment 1*, individual response surface plots for two animals and the average plot across six subjects are shown in Fig. 9.

It is readily apparent from inspection of the response surfaces that the patterns are highly repeatable from subject-to-subject and that each odor results in a unique pattern (Fig. 9). Some animal-to-animal variability does exist, as can be seen comparing the average plot and individual surfaces for acetophenone (Fig. 9*A*), but this does not diminish these conclusions. The amount of relief in the surface plots for each odors is perhaps striking with "hot spots" of high relative responsiveness neighboring "cold spots" of low relative responsiveness. This observation was confirmed by calculating the coefficients of variation (CV) of mean EOG responses along the rostrocaudal and dorsoventral grid lines, which were found to be similar for each axis (data not shown).

Finally, while the goal of *experiment 3* was to compare the two-dimensional OE response pattern on the septum across different odors, an unexpected result was documented with respect to the responsiveness of the septum vs. the turbinates. By pooling the responses from all recording locations on each turbinate and the septum to allow a comparison of their grand means, it is apparent that the septum is far less responsive to each of the three odorants than any of the turbinates (Fig. 10; see legend for statistical results). Since this comparison was suggested by the data and pooling across locations was ad hoc, statistical results should be judged with caution. However, the magnitude of the differences justifies the provisional inference that the septum is only fractionally as responsive to odorants as the turbinates. This comparatively low responsiveness is interesting given that CFD simulations show some of the highest odorant fluxes along the septum. That this difference was not a function of the inclusion of unresponsive zones on the septum was confirmed by comparisons of the largest individual recordings, which were all from turbinate locations (data not shown).

DISCUSSION

The sorption hypothesis. The field of olfaction, unlike the other sensory disciplines, lacks a basic understanding of the sensory array's layout. Indeed, since chemical sensing has no obvious spatial dimension, in contrast with vision or somatosensation, the very existence of a functional "map" in the OE has been challenged (Coppola et al. 2013). However, Adrian, one of the field's seminal investigators, suggested that olfaction, like the other special senses, may have a spatial component dependent on the sorption patterns that are set up as each odorant traverses the OE during respiration (Adrian 1942,

Fig. 7. Surface contours of odorant flux in the mouse nasal cavity from CFD simulations of the transport and deposition of acetophenone (*A*), isoamyl acetate (*B*), and nonane (*C*) at airflow rates typical of restful breathing (respiration) (A_i–C_i), 36 ml/min, and sniffing (A_{ii}–C_{ii}), 100 ml/min. *Left* and *middle* columns show the nasal cavity viewed from lateral and medial perspectives, respectively. *Right* column shows a truncated medial view of the olfactory recess with the septum removed. Note that the odorant flux in the olfactory recess is markedly nonuniform for acetophenone (*A*) and isoamyl acetate (*B*), but it is substantially uniform across the OE for nonane (*C*). Also note that the higher flow rate corresponding to sniffing moves the odor deposition patterning farther along the airflow path (see Fig. 6), compared with the slower respiratory flow rate case, for acetophenone (compare A_i with A_{ii}) and isoamyl acetate (compare B_i with B_{ii}). Finally note that the values of odorant flux vary by more than 2 orders of magnitude for the different odorants.

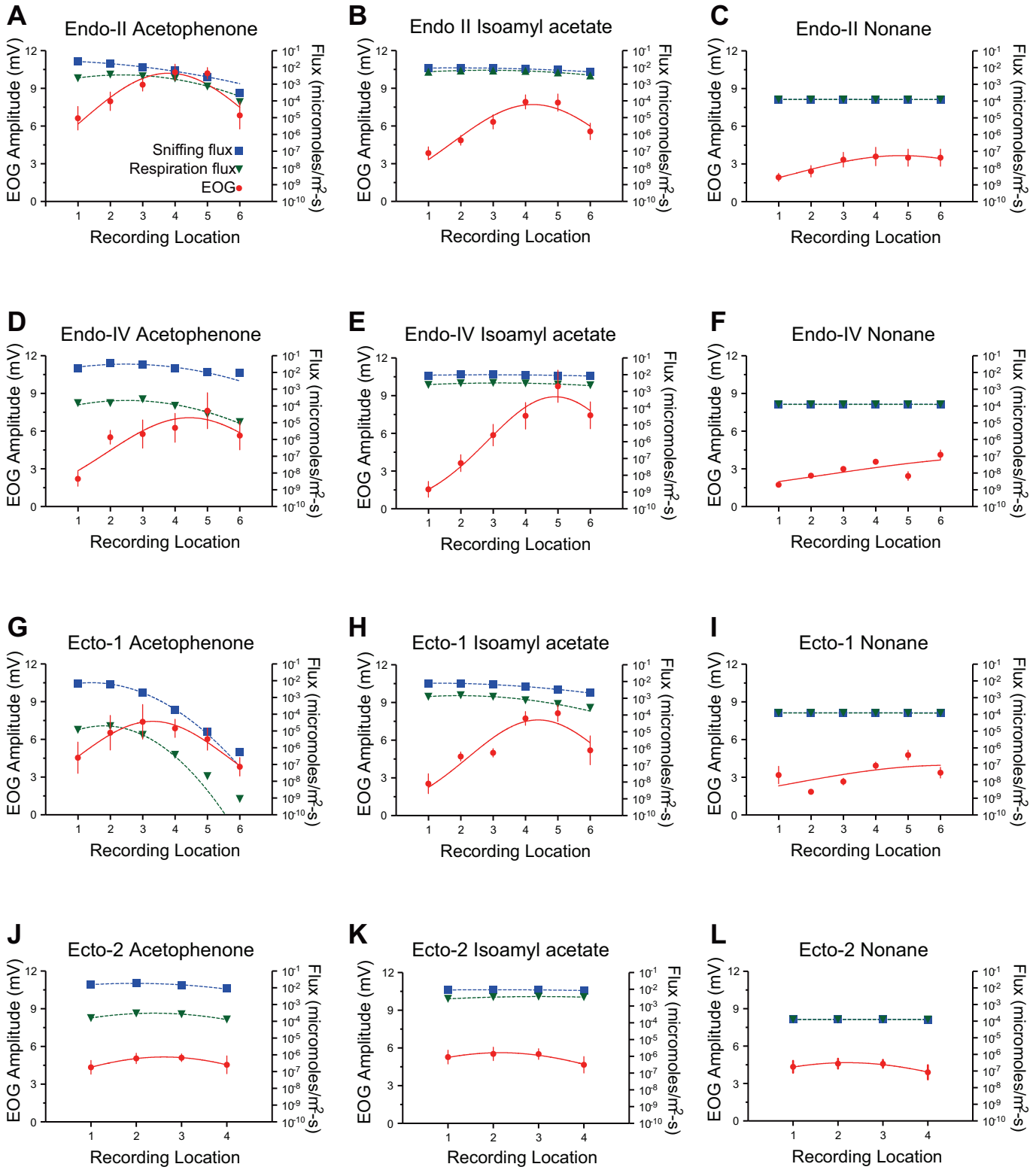

Fig. 8. Mean (± SE) EOG amplitudes at different recording locations (see Fig. 1) for 3 odorants (columns), acetophenone, isoamyl acetate, and nonane, on 4 turbinates (rows) are shown with red lines and symbols (see ANOVA results in Table 1). Since nonane was such a weak stimulus, a 5% vol/vol concentration was used while a 0.1% vol/vol solution was used for the other 2 odorants. Linear regressions R^2 and corresponding P values are provided in Table 2. Note that with the exception of ectoturbinate 2 the general trend was for a significant positive regression slope moving from caudal (1) to rostral (6) recording locations though some slopes were not significantly different. For comparison with the EOG responses, odorant flux values at the same approximate locations from the CFD simulations of odorant deposition (see Fig. 7) are plotted on separate logarithmic vertical axes (*right*) in green for the respiratory airflow rate and in blue for the sniffing airflow rate. Pearson r correlations and P values are provided in Table 2.

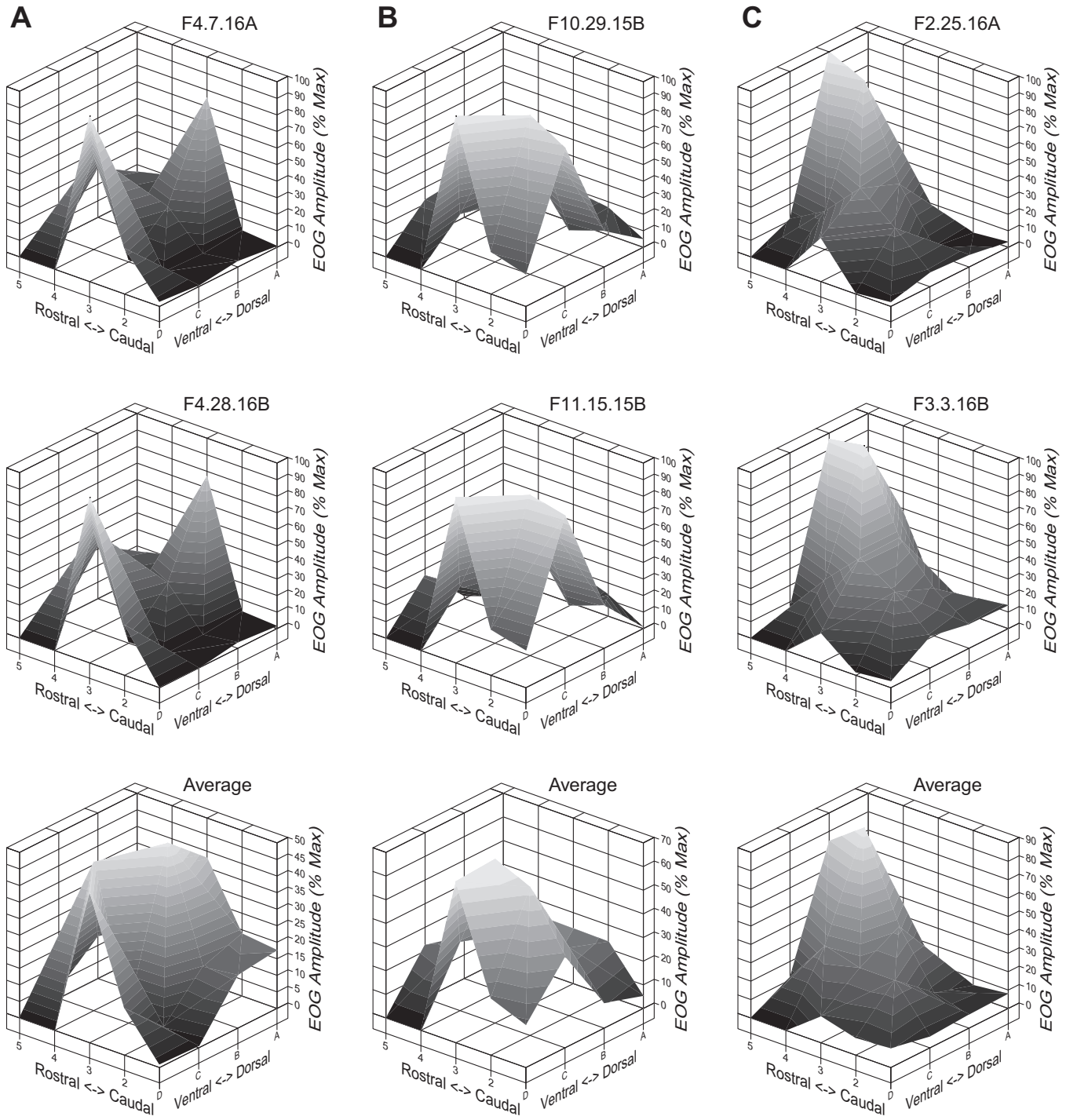

Fig. 9. Surface plots of raw EOG responses across 18 septal recording locations are shown for 2 individual animals (*top* and *middle rows*) and an averaged plot of 6 subjects (*bottom row*). Each column represents a different stimulus: *A*: highly soluble odorant acetophenone. *B*: moderately soluble isoamyl acetate. *C*: insoluble nonane. The *x*-axis and *y*-axis represent the rostrocaudal and dorsoventral planes, respectively (see Fig. 1), while the *z*-axis depicts EOG amplitudes as a percent of the maximum response for each subject. Max, maximum. Note: odors create highly characteristic response surfaces, often with multiple peaks.

1950, 1954). This idea and its subsequent elaborations have enjoyed both support and controversy in the decades since it was first proposed (cf. Cenier et al. 2013; Coppola et al. 2014; Courtiol et al. 2014; Rojas-Líbano and Kay 2012).

Our primary goal in this study was to test what we consider to be the central tenet of the sorption hypothesis: that olfactory receptors are spatially distributed across the OE so as to utilize the "chromatographic" separation of odorants during olfactory sampling (Schoenfeld and Cleland 2005, 2006; Scott 2006). This has been termed the "inherent pattern" of olfactory receptor distribution (Moulton 1976). We identify this assertion of the hypothesis as the most probative given that another key tenet of the sorption hypothesis—that there is chromatographic separation as odors move across the olfactory mucosa (Mozell 1964, 1966, 1970)—is an unavoidable outcome of physical chemistry, needing no further experimental support. That is,

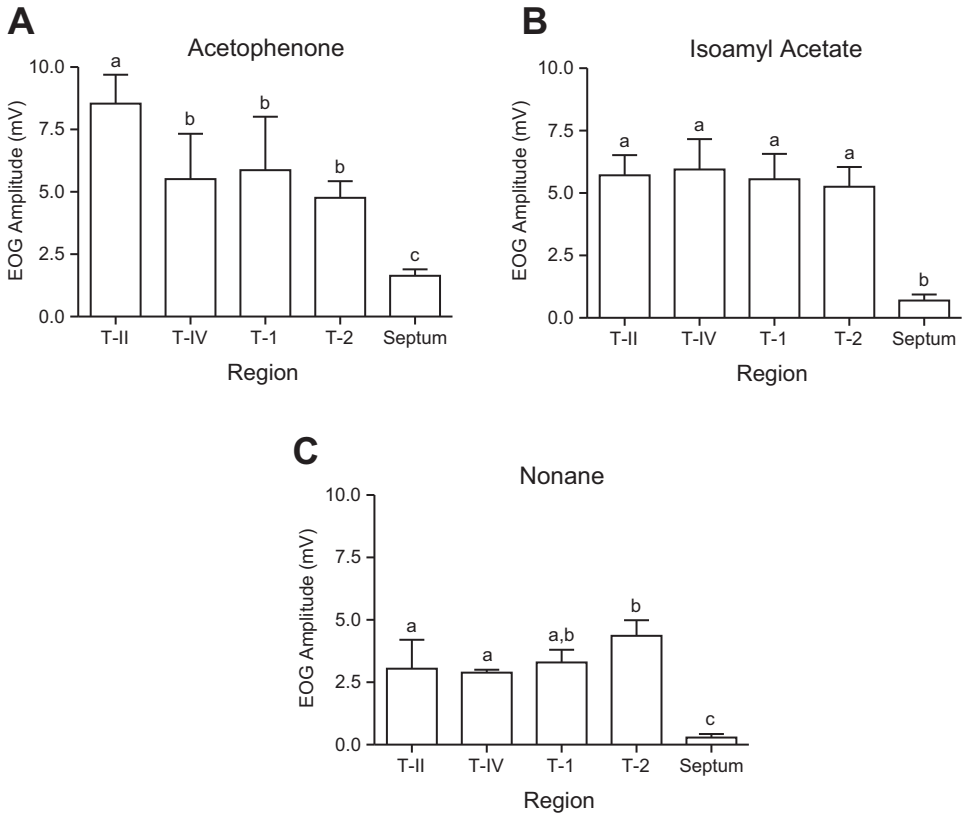

Fig. 10. Mean (± SE) EOG amplitudes from different turbinates or the septum with data pooled across locations. Each graph shows the results using a different stimulus. *A*: acetophenone (ANOVA, $F_{4,42} = 13.33$; $P < 0.0001$). *B*: isoamyl acetate (ANOVA, $F_{4,42} = 13.14$; $P < 0.0001$). *C*: nonane (ANOVA, $F_{4,42} = 20.02$; $P < 0.0001$). Within each graph, columns with the same letter above are not statistically different by Wilcoxon Tukey's multiple-comparison test.

chromatographic separation as odors pass through the moist nasal cavity is a necessary but not sufficient condition for any purported olfactory coding mechanism that is based on sorption.

The clearest prediction concerning the proposed inherent pattern of olfactory receptors is that one should find differential sensitivities when upstream or high-airflow regions of the OE are compared with downstream or low-airflow regions owing to the expected differential access to these regions by odors of different sorptiveness (Scott 2006; p. 126). By contrast, our earlier study of the mouse OE's inherent response map found little support for this prediction or the associated olfactory-fovea idea (Coppola et al. 2013). For example, mean EOG response profiles were not markedly different when we compared highly soluble benzaldehyde with highly insoluble nonane in upstream and downstream portions of the OE. And dorsal-central OE responses, generally, were not markedly different from peripheral OE responses. However, this previous study only targeted medial locations on the OE and utilized a relatively small stimulus set. Also, the limited published data on mouse nasal airflow forced us to make certain assumptions about flow patterns in the olfactory region that turn out to be inaccurate (see below).

In the present study, we expanded our sampling locations on the OE to include lateral turbinates, which are downstream in the airflow path and where the CFD simulations show relatively slow airflows. We used a larger set of odorants including many at the extremes of sorptiveness measured by mucus solubility (Kurtz et al. 2004; Scott et al. 2014). Finally, we performed CFD simulations of nasal airflow and odorant deposition in the mouse at flow rates typical of restful breathing and sniffing.

The results of *experiment 1* provide compelling evidence that the sensitivity profile of the dorsal-central OE differs from that of the peripheral OE in the mouse, in apparent agreement with the sorption hypothesis. Significantly greater mean EOG responses were recorded for eight of the 10 highly soluble odorants used as stimuli comparing a dorsomedial-central recording location to either a ventromedial- or dorsolateral-peripheral recording location (Fig. 4). And for the other two members of the soluble group of odors the mean central location response was significantly greater than one or the other peripheral locations. Averaging across all the odorants in the soluble group, the difference between the central location responses and the mean of the two peripheral location responses was 51.1% (range 11–94%).

Members of the odor set in *experiment 1* were chosen because they had been used as extremes of the solubility scale in a recent study of the sorption hypothesis in the rat (Scott et al. 2014). In this EOG-based study, medial-central responses were generally larger than peripheral responses for soluble odorants with the opposite true for insoluble odorants. These findings are in agreement with earlier demonstrations in frogs (Mozell 1964, 1966, 1970) and rats (Scott 2006; Scott et al. 1996, 1999; Scott et al. 2000) of a central vs. peripheral difference in responsiveness to mucus-soluble odorants.

By contrast, in the present study dorsal-central and peripheral recording locations tended to give similar responses for all the insoluble odorants. Three of the 10 insoluble odorants showed no statistical differences between recording locations and the central recording location was never the least responsive. For seven of the 10 insoluble odors the dorsolateral-peripheral recording location evidenced significantly greater responses than the ventromedial-peripheral locations (mean

39.3%, range 23–53%). This result was unexpected because *1*) according to the available OR gene-localization data the two peripheral locations should share more OR genes than either share with the central location (Fig. 1*C*; Iwema et al. 2004; Miyamichi et al. 2005; Ressler et al. 1993; Sullivan et al. 1996) and *2*) both peripheral locations are thought to be similar in their relative position along the olfactory pathway (Scott et al. 2014).

Experiment 2, which sampled adjacent recording locations along four different turbinates, demonstrated a marked rostral-greater to caudal-lesser gradient of response for all three odorants in three of the four turbinates examined. By contrast, the short ectoturbinate 2 tended to have flat EOG profiles for all three odorants tested. For some of the other turbinates, the anterior-posterior gradient was manifest in a more than twofold change in response upon an electrode movement of only 0.5 mm (Fig. 8). This finding replicates and extends to peripheral regions an observation made in our earlier OE mapping study (Coppola et al. 2013).

Can this anterior-posterior response gradient be explained—in the evolutionary sense—by the sorption hypothesis, i.e., a selective advantage of positioning ORs in the OE where they have the greatest exposure to their corresponding odotypes? Despite the central/peripheral dichotomy evidenced in *experiment 1*, the data from *experiment 2* suggest not. There were no statistically significant (or even borderline) correlations, positive or negative, between sorption values and mean EOGs for any odor-turbinate combination. In fact, where there was a substantial sorption gradient across a given turbinate it often had the opposite sign from the EOG gradient slopes for the same turbinate.

These data stand in marked contrast to EOG studies by Scott and colleagues in rats which have repeatedly shown decreasing responses to soluble odorants as recording locations are moved along the airstream path from more caudal to more rostral positions on the medial face of endoturbinate IV, a common target of previous studies (Scott 2006; Scott et al. 2014). The fact that the mouse sorption gradients are uncorrelated with EOG gradients of response along the same trajectory raises serious doubts about the validity of the sorption hypothesis in the mouse, at least along individual turbinates where the majority of evidence in favor of the hypothesis has been found in the rat (Scott 2006; Scott et al. 2014; Scott and Brierley 1999).

Moreover, the results from *experiments 2* (Fig. 8) and *3* (Fig. 10) show that the relatively soluble odorants acetophenone and isoamyl acetate were much stronger stimuli for all turbinates and recording locations, undoubtedly because of their air-mucus partition coefficients. To obtain response magnitudes that could be plotted on similar scales, we used a 50-fold higher concentration of nonane than the concentration for the other two odorants. Thus, in absolute terms, peripherally situated recording locations were more sensitive to soluble odorants than to the insoluble odor nonane, a fact also at odds with the sorption hypothesis which posits that the periphery should be more sensitive to insoluble odorants (Scott 2006; Scott et al. 2014).

Since the sorption hypothesis fails as an explanatory framework, what other phenomena exist in the OE that might correlate with the anterior-posterior response gradient observed across most turbinates? Recently, it has been demonstrated that OSNs located dorsally and anteriorly on the septal OE have longer cilia, higher adenylyl cyclase (AC_{III}) concentrations, and greater sensitivity to odors than their more ventrally located counterparts (Challis et al. 2015). However, the correlation between anterior-posterior axis location and cilia length/sensitivity reported by Challis and associates did not extend to the turbinates, where we consistently observed marked response gradients. Indeed, the turbinates, where cilia are comparatively short and uniform, produced mean OE responses that were typically eightfold higher than those from the septum, where cilia are long dorsally and anteriorly (cf. our Fig. 8 with Challis et al. 2015, Figure S1).

Importantly, the anterior-posterior gradient in EOG responses reported here may not have its origins in the two-dimensional distribution of ORs in OSNs. As pointed out by Scott (2006), spatial patterns of mucosal thickness, or the concentration of olfactory chaperones, enzymes or modulators could all contribute to regional differences in the EOG responses, though we are unaware of evidence suggesting an anterior-posterior gradient in any of these factors.

Whatever the origin of the prominent anterior-posterior gradient of responses in the OE, the conflicting findings of *experiments 1* and *2* require further interpretation. One explanation for these disparate results is that *experiment 1* is evidence of a "global" or dichotomous sorption effect (i.e., comparing the dorsal-central region to the rest of the OE) and *experiment 2* is evidence against any "local" sorption effect (i.e., within a turbinate). However, why sorption gradients of similar magnitudes would be correlated with responsivity maps across regions but not within a turbinate is hard to square with the sorption hypothesis. As an alternative to this hypothesis, the results of *experiment 1*—and perhaps other studies demonstrating central-peripheral differences in OE responsivity—may be more parsimoniously explained by the growing body of evidence that the OE can be divided into nonoverlapping dorsal (central) and a ventral (peripheral) zones, a dichotomy initially recognized on the basis of zone-specific markers (Kobayakawa et al. 2007). In mice, virtually all of the phylogenetically identified Class I ORs are located in the dorsal zone while Class II ORs are expressed in both zones (Niimura and Nei 2007). Class I ORs tend to have water-soluble ligands (Saito et al. 2009). However, recent evidence suggests that the dorsal zone–ventral zone dichotomy may only secondarily be related to the water solubility of ligands for the ORs found in these locations. Rather, these regions of the OE seem to represent two functional channels: the central zone for transmitting hard-wired aversive odorant information and the peripheral OE functioning in olfactory learned behaviors (Kobayakawa et al. 2007). Adding to this line of reasoning, Class I receptors are more evolutionarily conserved and seem to be under different selective pressures than the Class II receptors, the latter far outnumbering the former (Niimura 2014).

Thus our observation that the dorsal zone of the OE is more responsive to sorptive odorants than either of the peripheral recording locations (*experiment 1*) may simply reflect an evolutionary contingent state—i.e., we propose that OR subfamilies with water-soluble ligands expanded first in the semiterrestrial forerunners of fully terrestrial mammals and OR subfamilies with insoluble ligands were added later, forcing nasal cavity expansion, as mammals occupied ever more xeric environs where these receptors would confer an adaptive advan-

tage. Whatever the explanation for the results of *experiment 1*, it is clearly the case that both central and peripheral areas of the mouse OE respond vigorously, though not equally, to both soluble and insoluble odorants. Apart from our data on this point (see Fig. 4), Sato and colleagues (2015) have recently shown that transgenic mice lacking all their dorsal area receptors (ΔD mice) have thresholds identical to wild type for certain highly water-soluble substances and ΔD mice can detect one of the enantiomers of the soluble odorant carvone down to 10^{-15}% (wt/wt). Finally, while Class I receptors, which are limited in distribution to the dorsal (central) region, may have water-soluble ligands, Class II receptors found everywhere in the OE, outnumber Class I receptors dorsally. These factors defy any simple dichotomy between phylogenetic class of receptor, position in the OE, and ligand sorptiveness (Niimura and Nei 2007).

Another facile assumption of the sorption hypothesis is brought into question by a careful inspection of airflow patterns from our CFD simulations. It is oft stated that the nasal airflow pattern in rodents appears to match the distribution pattern of many olfactory receptors consistent with a sorption-based olfactory process (Schoenfeld and Cleland 2005; Scott 2006; Scott et al. 2014). However, the airflow patterns over and around the olfactory turbinates are more complex than previously appreciated with flow streamlines oriented parallel or tangential to OR zonal boundaries as frequently as they are perpendicular (cf. Fig. 1*A* vs. Fig. 6, A_i and A_{ii}). Further complicating matters are the differential flow speeds across the nasal cavity created by such low-resistance channels as the dorsal meatus. This latter feature ensures that odor-laden inspired air is channeled directly to the caudal aspect of the dorsal turbinates with minimal upstream filtering (Fig. 6, B_i and B_{ii}).

Taken together, neither our analysis of the intrinsic patterns of olfactory responsivity and their relationship to specific odorant fluxes nor our simulated airflow patterns support a localized sorption based olfactory process in the mouse such as that codified in the sorption hypothesis (Schoenfeld and Cleland 2005, 2006). However, the results of *experiment 1* leave open the possibility of a global sorption effect—i.e., one contrasting the dorsal-central region with the remainder of the OE.

The olfactory fovea hypothesis. A related hypothesis known as the zonation or olfactory "fovea" hypothesis, which draws an analogy between the retinal fovea and olfaction could act independently of a sorption-based coding mechanism (Schoenfeld and Cleland 2005, 2006). The hypothesis in its simplest form asserts that ". . . animals could adjust their sniffing to direct particular odotopes to the most responsive ORNs, particularly when such ORNs are positioned in areas not well matched for the intrinsic sorptiveness of the odorant" (Schoenfeld and Cleland 2005). This hypothesis requires *1*) that there is differential placement of ORs in the OE based on the sorptiveness of their ligands and *2*) that mammals—at least—have the ability to direct the delivery of odors with different sorptiveness to the appropriate areas of the nasal cavity by varying sniffing behavior. Our data support the first tenet of the hypothesis in so far as we consistently found greater sensitivity for water-soluble odorants on the dorsally-centrally located endoturbinate II_d compared with the peripherally located endoturbinate IV and ectoturbinate 1 (Fig. 4). However, we did not find any area of the OE that particularly favored insoluble odorants. Indeed, in *experiment 1*, endoturbinate II_d's mean responses were statistically indistinguishable from one or both of the peripheral recording locations for nine of the 10 insoluble odorants in our sample (Fig. 4). This latter finding and the flux simulation data that reveal negligible regional differences in sorption of the insoluble odorant nonane across the OE, at flow rates typical of respiration and sniffing, suggest there is no inspiratory strategy that would favor detection/discrimination of insoluble odorants (Figs. 7, C_i and C_{ii} and 8, *C*, *F*, *I*, and *L*).

Could mice use an inspiratory strategy to selectively direct soluble odorants to endoturbinate II_d where there appear to be more ORs with soluble odorant ligands given the results of *experiment 1*? Consider the flux data from our CFD simulation of the soluble odorant acetophenone (Fig. 6), and examine the odor flux contours (Fig. 7) and profiles along individual turbinates (Fig. 8). First, note that the higher the inspiratory flow rate—sniffing vs. respiration in our simulations—the more odorant that enters the nasal cavity and the higher the sorption. Thus a mouse encountering a potential odor source would do well to sniff no matter the sorptiveness of any odors to be found there, a confound with the zonation hypothesis that may be impossible to disentangle experimentally. Second, sniffing, which admittedly can counteract some upstream odor filtering by nonolfactory epithelium, actually tends to move the "hot spot" of sorption for acetophenone off of endoturbinate II_d to more peripheral turbinates (Fig. 7, A_i and A_{ii}). Notably, while acetophenone is not at the extreme of mucus solubility, for odorants tested in this study (−3.74 log air/mucus dilution coefficient, see Fig. 2), odorants with greater mucus solubility have very similar sorption pattern to acetophenone (Rygg et al. 2017). Finally, given that most natural "odor objects" are mixtures (Wilson and Stevenson 2003), likely possessing components with different sorptive characteristics, it is hard to envision any inspiratory strategy that would be more effective for one odor object compared with another.

Perhaps these considerations explain why the preponderance of published data on sniffing behavior in rodents do not support differential sniffing related to the sorptiveness of odorants. For example, Youngentob and colleagues (1987) failed to show any sorption effect when they compared sniffing toward moderately soluble isoamyl acetate and highly soluble pyridine. A more recent study in rats found "sniff strength" had a negligible effect on odor representation using bulbar optical imaging and found that behaving subjects did not modulate sniff flow rate to improve odor discrimination (Cenier et al. 2013). In yet another recent study that employed noninvasive whole-body plethysmography, rats did not alter sniff strength when the sorptiveness of odor targets were systematically altered in discrimination tests (Courtiol et al. 2014). However, Rojas-Líbano and Kay (2012), measuring respiratory activity through diaphragm electromyography in behaving rats, found differential sniffing parameters when rats were detecting "high-sorption" vs. "low-sorption" targets though the effects were quite small (explaining ~13% of the variance in sniffing). More importantly, these tests were confounded by marked overall differences in the difficulty of detecting low-sorption compared with high-sorption odorants.

Thus, with the exception of this latter study, there do not seem to be any other behavioral data in animals or perceptual data in humans that support the hypothesis that subjects vary

inspiratory parameters on the basis of odor sorptiveness (Schoenfeld and Cleland 2005, 2006). Rather, sniffing would appear to be a ubiquitous appetitive behavior employed whenever a novel object is encountered, even displayed with normal metrics in rodents lacking an olfactory bulb (Welker 1964). This fact resonates with first principles and our simulations of odorant sorption, which demonstrate that more molecules are brought into the nasal cavity and deposited during sniffing than during slow inspiration no matter an odorant's sorptiveness.

Septal response maps. The results of *experiment 3* (Fig. 7), which focused on mapping the odor responses from the septum, are reminiscent of previous attempts to record from this portion of the OE. Mackay-Sim and Kesteven (1994) using the EOG and Youngentob and colleagues (1995) using voltage-sensitive dye imaging reported odor-specific response patterns in rats that were repeatable across subjects and tended to have concentric peaks and valleys forming unique 3D surfaces. In particular, our results concur with these earlier reports in failing to show distinct zonal boundaries discernable across odor types. Our septal response maps did not show the rostral-larger to caudal-lesser gradient that was so prominent across three of the four turbinates (Fig. 4). In fact, the variability in response profiles along the ventral to dorsal axis were just as prominent as those along the rostral to caudal axis.

Though functional significance of the odor-specific septal response patterns is unclear, their reproducibility supports the conclusion that there are millimeter-scale features of the OE response maps that are detectable by an ensemble recording method like the EOG. At an even larger regional scale it was surprising, as noted above, that the septum produced much smaller responses than the turbinates to all three odors tested, especially given the former's central position in the inspiratory airstream and the high odor fluxes that occur there (Fig. 8; cf. Challis et al. 2015).

General conclusions. A dorsal-central recording location of the mouse OE displayed, on average, greater amplitude EOG responses to soluble odorants than did either of two peripheral recording locations, though there was no such regional specificity for highly insoluble odorants. This finding supports the sorption hypothesis insofar as sensitivity to and sorption of odotypes are correlated across two regions of the OE: dorsal-central and peripheral. However, point-to-point comparisons of EOG responses and CFD odorant flux simulations failed to show any correlation despite expansive sampling and the use of both respiratory-typical and sniffing-typical flow rates. Airflow paths through the nasal cavity obtained from CFD simulations were complex with little obvious correlation to reported OR zonal boundaries. Comparisons of odor flux patterns using respiratory-typical and sniffing-typical flow rates did not support the proposition that subjects could adjust sniffing parameters to deliver odorants of a particular sorption class to selected regions of the OE.

In contrast to these findings, a pronounced caudal-lesser to rostral-greater gradient of EOG average magnitudes was observed across most olfactory turbinates in response to odors that varied by sorptiveness. In the area of the nasal septum, EOG recordings at regular grid locations demonstrated odor specific and highly repeatable response surfaces. However, the overall responsiveness of the septum was nearly an order of magnitude smaller than that observed in the olfactory turbinates despite experiencing some of the highest airflow rates based on our CFD simulations.

Collectively, these results cast doubt on the sorption and zonation hypotheses in the mouse but confirm large regional differences in responsivity at the ensemble-recording level whose role in olfaction, if any, remains to be explained. It is proposed that the regional differences in OE response patterns of the mouse—and perhaps other macrosmatic mammals—may be an evolutionary contingent state devoid of the functional significance found in receptor array layouts of other sensory epithelia like the retina.

ACKNOWLEDGMENTS

Present address for B. A. Craven: Division of Applied Mechanics, Office of Science and Engineering Laboratories, Center for Devices and Radiological Health, U.S. Food and Drug Administration, Silver Spring, Maryland.

GRANTS

This work was supported by grants from the National Science Foundation (IOS-1655113 to D. M. Coppola. and IOS-1120375 to B. A. Craven) and the Chenery Endowment to D. M. Coppola.

DISCLOSURES

No conflicts of interest, financial or otherwise, are declared by the authors.

AUTHOR CONTRIBUTIONS

D.M.C. and B.A.C. conceived and designed research; D.M.C., B.E.R., and B.A.C. performed experiments; D.M.C., B.E.R., and B.A.C. analyzed data; D.M.C., B.E.R., and B.A.C. interpreted results of experiments; D.M.C. and B.A.C. prepared figures; D.M.C. and B.A.C. drafted manuscript; D.M.C., B.E.R., and B.A.C. edited and revised manuscript; D.M.C., B.E.R., and B.A.C. approved final version of manuscript.

REFERENCES

Adrian ED. Olfactory reactions in the brain of the hedgehog. *J Physiol* 100: 459–473, 1942. doi:10.1113/jphysiol.1942.sp003955.

Adrian ED. Sensory discrimination with some recent evidence from the olfactory organ. *Br Med Bull* 6: 330–332, 1950. doi:10.1093/oxfordjournals.bmb.a073625.

Adrian ED. The basis of sensation; some recent studies of olfaction. *BMJ* 1: 287–290, 1954. doi:10.1136/bmj.1.4857.287.

Barber CN, Coppola DM. Compensatory plasticity in the olfactory epithelium: age, timing, and reversibility. *J Neurophysiol* 114: 2023–2032, 2015. doi:10.1152/jn.00076.2015.

Catania KC. The sense of touch in the star-nosed mole: from mechanoreceptors to the brain. *Philos Trans R Soc Lond B Biol Sci* 366: 3016–3025, 2011. doi:10.1098/rstb.2011.0128.

Cenier T, McGann JP, Tsuno Y, Verhagen JV, Wachowiak M. Testing the sorption hypothesis in olfaction: a limited role for sniff strength in shaping primary odor representations during behavior. *J Neurosci* 33: 79–92, 2013. doi:10.1523/JNEUROSCI.4101-12.2013.

Challis RC, Tian H, Wang J, He J, Jiang J, Chen X, Yin W, Connelly T, Ma L, Yu CR, Pluznick JL, Storm DR, Huang L, Zhao K, Ma M. An olfactory cilia pattern in the mammalian nose ensures high sensitivity to odors. *Curr Biol* 25: 2503–2512, 2015. doi:10.1016/j.cub.2015.07.065.

Coppola DM, Craven BA, Seeger J, Weiler E. The effects of naris occlusion on mouse nasal turbinate development. *J Exp Biol* 217: 2044–2052, 2014. doi:10.1242/jeb.092940.

Coppola DM, Waggener CT, Radwani SM, Brooks DA. An electroolfactogram study of odor response patterns from the mouse olfactory epithelium with reference to receptor zones and odor sorptiveness. *J Neurophysiol* 109: 2179–2191, 2013. doi:10.1152/jn.00769.2012.

Courtiol E, Lefèvre L, Garcia S, Thévenet M, Messaoudi B, Buonviso N. Sniff adjustment in an odor discrimination task in the rat: analytical or synthetic strategy? *Front Behav Neurosci* 8: 145, 2014. doi:10.3389/fnbeh.2014.00145.

Craven BA, Neuberger T, Paterson EG, Webb AG, Josephson EM, Morrison EE, Settles GS. Reconstruction and morphometric analysis of the nasal airway of the dog (*Canis familiaris*) and implications regarding olfactory airflow. *Anat Rec (Hoboken)* 290: 1325–1340, 2007. doi:10.1002/ar.20592.

Craven BA, Paterson EG, Settles GS, Lawson MJ. Development and verification of a high-fidelity computational fluid dynamics model of canine nasal airflow. *J Biomech Eng* 131: 091002, 2009. doi:10.1115/1.3148202.

Iwema CL, Fang H, Kurtz DB, Youngentob SL, Schwob JE. Odorant receptor expression patterns are restored in lesion-recovered rat olfactory epithelium. *J Neurosci* 24: 356–369, 2004. doi:10.1523/JNEUROSCI.1219-03.2004.

Kent PF, Mozell MM, Murphy SJ, Hornung DE. The interaction of imposed and inherent olfactory mucosal activity patterns and their composite representation in a mammalian species using voltage-sensitive dyes. *J Neurosci* 16: 345–353, 1996.

Kobayakawa K, Kobayakawa R, Matsumoto H, Oka Y, Imai T, Ikawa M, Okabe M, Ikeda T, Itohara S, Kikusui T, Mori K, Sakano H. Innate versus learned odour processing in the mouse olfactory bulb. *Nature* 450: 503–508, 2007. doi:10.1038/nature06281.

Kurtz DB, Zhao K, Hornung DE, Scherer P. Experimental and numerical determination of odorant solubility in nasal and olfactory mucosa. *Chem Senses* 29: 763–773, 2004. doi:10.1093/chemse/bjh079.

Lawson MJ, Craven BA, Paterson EG, Settles GS. A computational study of odorant transport and deposition in the canine nasal cavity: implications for olfaction. *Chem Senses* 37: 553–566, 2012. doi:10.1093/chemse/bjs039.

Login H, Håglin S, Berghard A, Bohm S. The stimulus-dependent gradient of Cyp26B1+ olfactory sensory neurons is necessary for the functional integrity of the olfactory sensory map. *J Neurosci* 35: 13807–13818, 2015. doi:10.1523/JNEUROSCI.2247-15.2015.

Mackay-Sim A, Kesteven S. Topographic patterns of responsiveness to odorants in the rat olfactory epithelium. *J Neurophysiol* 71: 150–160, 1994.

Miyamichi K, Serizawa S, Kimura HM, Sakano H. Continuous and overlapping expression domains of odorant receptor genes in the olfactory epithelium determine the dorsal/ventral positioning of glomeruli in the olfactory bulb. *J Neurosci* 25: 3586–3592, 2005. doi:10.1523/JNEUROSCI.0324-05.2005.

Motulski H. GraphPad Software (November 7, 2016). https://www.graphpad.com.

Moulton DG. Spatial patterning of response to odors in the peripheral olfactory system. *Physiol Rev* 56: 578–593, 1976.

Mozell MM. Evidence for sorption as a mechanism of the olfactory analysis of vapours. *Nature* 203: 1181–1182, 1964. doi:10.1038/2031181a0.

Mozell MM. The spatiotemporal analysis of odorants at the level of the olfactory receptor sheet. *J Gen Physiol* 50: 25–41, 1966. doi:10.1085/jgp.50.1.25.

Mozell MM. Evidence for a chromatographic model of olfaction. *J Gen Physiol* 56: 46–63, 1970. doi:10.1085/jgp.56.1.46.

Niimura Y. Olfactory receptor genes: evolution. *eLS, Wiley Online Library* (August 15, 2014). doi: 10.1002/9780470015902.a0020789.pub2.

Niimura Y, Nei M. Extensive gains and losses of olfactory receptor genes in mammalian evolution. *PLoS One* 2: e708, 2007. doi:10.1371/journal.pone.0000708.

Osterberg G. Topography of the layer of rods and cones in the human retina. *Acta Ophthalmol Suppl* 6: 1–103, 1935.

Ranslow AN, Richter JP, Neuberger T, Van Valkenburgh B, Rumple CR, Quigley AP, Pang B, Krane MH, Craven BA. Reconstruction and morphometric analysis of the nasal airway of the white-tailed deer (Odocoileus virginianus) and implications regarding respiratory and olfactory airflow. *Anat Rec (Hoboken)* 297: 2138–2147, 2014. doi:10.1002/ar.23037.

Ressler KJ, Sullivan SL, Buck LB. A zonal organization of odorant receptor gene expression in the olfactory epithelium. *Cell* 73: 597–609, 1993. doi:10.1016/0092-8674(93)90145-G.

Rojas-Líbano D, Kay LM. Interplay between sniffing and odorant sorptive properties in the rat. *J Neurosci* 32: 15577–15589, 2012. doi:10.1523/JNEUROSCI.1464-12.2012.

Rygg AD, Van Valkenburgh B, Craven BA. The influence of sniffing on airflow and odorant deposition in the canine nasal cavity. *Chem Senses* 42: 683–698, 2017. doi:10.1093/chemse/bjx053.

Saito H, Chi Q, Zhuang H, Matsunami H, Mainland JD. Odor coding by a Mammalian receptor repertoire. *Sci Signal* 2: ra9, 2009. doi:10.1126/scisignal.2000016.

Sato T, Kobayakawa R, Kobayakawa K, Emura M, Itohara S, Kizumi M, Hamana H, Tsuboi A, Hirono J. Supersensitive detection and discrimination of enantiomers by dorsal olfactory receptors: evidence for hierarchical odour coding. *Sci Rep* 5: 14073, 2015. doi:10.1038/srep14073.

Schoenfeld TA, Cleland TA. The anatomical logic of smell. *Trends Neurosci* 28: 620–627, 2005. doi:10.1016/j.tins.2005.09.005.

Schoenfeld TA, Cleland TA. Anatomical contributions to odorant sampling and representation in rodents: zoning in on sniffing behavior. *Chem Senses* 31: 131–144, 2006. doi:10.1093/chemse/bjj015.

Scott JW. Sniffing and spatiotemporal coding in olfaction. *Chem Senses* 31: 119–130, 2006. doi:10.1093/chemse/bjj013.

Scott JW, Brierley T. A functional map in rat olfactory epithelium. *Chem Senses* 24: 679–690, 1999. doi:10.1093/chemse/24.6.679.

Scott JW, Brierley T, Schmidt FH. Chemical determinants of the rat electro-olfactogram. *J Neurosci* 20: 4721–4731, 2000.

Scott JW, Davis LM, Shannon D, Kaplan C. Relation of chemical structure to spatial distribution of sensory responses in rat olfactory epithelium. *J Neurophysiol* 75: 2036–2049, 1996.

Scott JW, Sherrill L, Jiang J, Zhao K. Tuning to odor solubility and sorption pattern in olfactory epithelial responses. *J Neurosci* 34: 2025–2036, 2014. doi:10.1523/JNEUROSCI.3736-13.2014.

Suga N, Simmons JA, Jen PH. Peripheral specialization for fine analysis of doppler-shifted echoes in the auditory system of the "CF-FM" bat *Pteronotus parnellii*. *J Exp Biol* 63: 161–192, 1975.

Sullivan SL, Adamson MC, Ressler KJ, Kozak CA, Buck LB. The chromosomal distribution of mouse odorant receptor genes. *Proc Natl Acad Sci USA* 93: 884–888, 1996. doi:10.1073/pnas.93.2.884.

Waggener CT, Coppola DM. Naris occlusion alters the electro-olfactogram: evidence for compensatory plasticity in the olfactory system. *Neurosci Lett* 427: 112–116, 2007. doi:10.1016/j.neulet.2007.09.013.

Welker WI. Analysis of sniffing in the albino rat. *Behaviour* 22: 223–244, 1964. doi:10.1163/156853964X00030.

Wilson DA, Stevenson RJ. Olfactory perceptual learning: the critical role of memory in odor discrimination. *Neurosci Biobehav Rev* 27: 307–328, 2003. doi:10.1016/S0149-7634(03)00050-2.

Youngentob SL, Kent PF, Sheehe PR, Schwob JE, Tzoumaka E. Mucosal inherent activity patterns in the rat: evidence from voltage-sensitive dyes. *J Neurophysiol* 73: 387–398, 1995.

Youngentob SL, Mozell MM, Sheehe PR, Hornung DE. A quantitative analysis of sniffing strategies in rats performing odor detection tasks. *Physiol Behav* 41: 59–69, 1987. doi:10.1016/0031-9384(87)90131-4.